JACS
JOURNAL OF THE AMERICAN CHEMICAL SOCIETY
Article
pubs.acs.org/JACS

Diniobium Inverted Sandwich Complexes with μ-η^6:η^6-Arene Ligands: Synthesis, Kinetics of Formation, and Electronic Structure

Thomas L. Gianetti,[†] Grégory Nocton,[†,‡] Stefan G. Minasian,[§,∥] Neil C. Tomson,[†] A. L. David Kilcoyne,[⊥] Stosh A. Kozimor,[∥] David K. Shuh,[§] Tolek Tyliszczak,[⊥] Robert G. Bergman,*[,†] and John Arnold*[,†]

[†]Department of Chemistry, University of California, Berkeley, California 94720, United States
[‡]Laboratoire Hétéroéléments et Coordination, UMR CNRS 7653, Ecole Polytechnique, 91128 Palaiseau, France
[§]Chemical Sciences Division and [⊥]Advanced Light Source, Lawrence Berkeley National Laboratory, Berkeley, California 94720, United States
[∥]Chemistry Division, Los Alamos National Laboratory, Los Alamos, New Mexico 87545, United States

Supporting Information

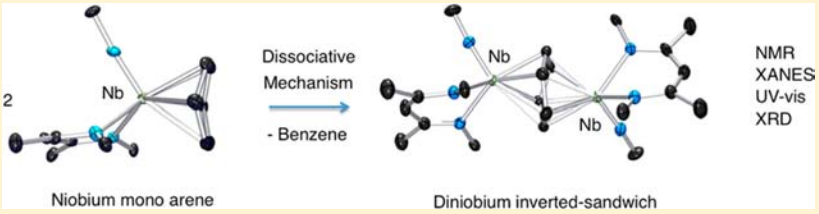

ABSTRACT: Monometallic niobium arene complexes [Nb(BDI)(N^tBu)(R-C_6H_5)] (**2a**: R = H and **2b**: R = Me, BDI = *N*,*N*′-diisopropylbenzene-β-diketiminate) were synthesized and found to undergo slow conversion into the diniobium inverted arene sandwich complexes [[(BDI)Nb(N^tBu)]$_2$(μ-RC_6H_5)] (**7a**: R = H and **7b**: R = Me) in solution. The kinetics of this reaction were followed by ^{1}H NMR spectroscopy and are in agreement with a dissociative mechanism. Compounds **7a**-**b** showed a lack of reactivity toward small molecules, even at elevated temperatures, which is unusual in the chemistry of inverted sandwich complexes. However, protonation of the BDI ligands occurred readily on treatment with [H(OEt_2)][B(C_6F_5)$_4$], resulting in the monoprotonated cationic inverted sandwich complex **8** [[(BDI$^{\#}$)Nb(N^tBu)][(BDI)Nb(N^tBu)](μ-C_6H_5)][B(C_6F_5)$_4$] and the dicationic complex **9** [[(BDI$^{\#}$)Nb(N^tBu)]$_2$(μ-RC_6H_5)][B(C_6F_5)$_4$]$_2$ (BDI$^{\#}$ = (ArNC(Me))$_2$$CH_2$). NMR, UV−vis, and X-ray absorption near-edge structure (XANES) spectroscopies were used to characterize this unique series of diamagnetic molecules as a means of determining how best to describe the Nb−arene interactions. The X-ray crystal structures, UV−vis spectra, arene ^{1}H NMR chemical shifts, and large J_{CH} coupling constants provide evidence for donation of electron density from the Nb d-orbitals into the antibonding π system of the arene ligands. However, Nb $L_{3,2}$-edge XANES spectra and the lack of sp^3 hybridization of the arene carbons indicate that the Nb → arene donation is not accompanied by an increase in Nb formal oxidation state and suggests that $4d^2$ electronic configurations are appropriate to describe the Nb atoms in all four complexes.

INTRODUCTION

Arene complexes of low-valent metal ions are an intriguing class of molecules because of the high variability in metal−arene interactions.[1−3] Facially bound arene ligands are known to bind to a wide range of metals in unusual oxidation states using a variety of bonding modes. In 1983, Krüger et al. reported the first dinuclear C_6H_6 complex, in which a benzene ligand was bound by two CpV moieties in a μ-η^6:η^6 fashion.[4] Although the inverted arene sandwich motif remains very rare, similar molecules have been found with s-,[5] d-,[4,6−12] and f-block[13−24] metal ions. Typically, these molecules are synthesized by the reduction of metal−halide precursors in aromatic solvents. Upon formation of electron-rich metal centers, coordination of an aromatic solvent molecule provides chemical stability by mixing of the occupied metal d-manifold with the vacant π system of the arene ring. Important questions remain, however, regarding the bonding in these compounds, such as how to assign formal oxidation states and how electron density is shared between the metal and the arene. Support for reduction of the arene to form an anionic ligand can be derived from detailed structural investigations, which have revealed elongation[4−24] of the average C−C distances and disruption of arene planarity.[6,7,9,10,13,16,17,19,20] However, evaluating arene charge based on these structural distortions can be challenging because both neutral[4,6−11] and anionic[5,12−24] configurations have been assigned previously.[25] In addition, questions regarding the mechanism of formation of these bimetallic complexes have not been resolved fully. In a report on the hafnium species $Hf_2I_4(PMe_2Ph)_2$(μ-η^6:η^6-arene), Cotton and co-workers proposed the intermediacy of the monometallic $HfI_2(PMe_2Ph)_2$(η^6-arene).[6] More recently, P. Arnold et al. provided computational and experimental evidence for

Received: December 10, 2012
Published: January 23, 2013

   dx.doi.org/10.1021/ja311966h | *J. Am. Chem. Soc.* 2013, 135, 3224−3236

Scheme 1. Synthesis of Complexes 2a−b

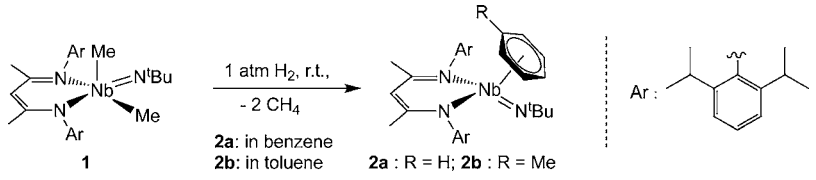

formation of U^{3+} inverted sandwich complexes via a monometallic arene intermediate.[23]

Recently, in an effort to explore the catalytic potential of low-valent niobium, we reported the catalytic, Z-selective hydrogenation of internal alkynes by the Nb(III) complex [Nb(BDI)(N^tBu)($CO)_2$] (**1**) (BDI = *N,N′*-2,6-diisopropylphenyl-*β*-diketiminate).[26] While performing these catalytic studies in aromatic solvents, we became intrigued by the observation of arene complexes. These complexes formed in the absence of CO, presumably by trapping a low-coordinate trivalent niobium complex "Nb(BDI)(N^tBu)", which was proposed to be an active species in the catalytic cycle. The study of low-valent, group V transition metals, such as Nb, could lead to new chemical transformations and catalytic processes. In earlier work, remarkable reactivity and redox behavior has been reported for monomeric low-valent Nb(III) complexes that were isolated or generated *in situ*, spanning activation of small molecules[27−32] hydrogenation,[26,33] C−C coupling,[34−38] and C−H bond activation reactions.[39−44] The study presented here describes the synthesis and characterization of several new Nb arene complexes, including the kinetics of formation of the first bimetallic μ-η^6:η^6-arene inverted sandwich complexes[45] from the parent monometallic species. Protonation of the BDI ligands afforded the mono- and dicationic μ-η^6:η^6-benzene complexes. All four inverted sandwich complexes were subjected to a suite of characterization methods, including single-crystal X-ray diffraction as well as UV−vis and Nb $L_{3,2}$-edge X-ray absorption near-edge structure (XANES) spectroscopies. Each of the four inverted sandwich complexes also bears a diamagnetic electronic configuration, which allowed an unusual opportunity to undertake an in-depth ^1H and ^{13}C (1D and 2D) NMR spectroscopic study of the metal−arene interactions. The combined experimental approach provides new insight into the electronic structure of d-block metal−arene complexes.

RESULTS AND DISCUSSION

Monometallic Arene Complexes. The Nb(V) complex [Nb(BDI)(N^tBu)Me_2][46] (**1**) reacts with H_2 in benzene or toluene at room temperature to form the complexes [Nb(BDI)(N^tBu)(R-C_6H_5)] (R = H, **2a** or Me, **2b**) as diamagnetic red powders in high purities and very good yields (93% and 91%, respectively, Scheme 1). Initial efforts to obtain X-ray quality crystals of **2a−b** were thwarted by their propensity to form mixtures with their bimetallic counterparts upon isolation (see below). Nevertheless, rapid crystallization of **2a** from a mixture of toluene/hexanes formed material suitable for X-ray crystallographic analysis (Figure 1, Tables 1 and S1). Although several niobium arene compounds have been reported,[47−62] to the best of our knowledge **2a** is the first niobium−benzene complex that has been structurally characterized. In **2a** the BDI and imido ligands occupy facial positions in a pseudo-octahedral geometry. The N−Nb−N angle of the BDI ligand is 81.4°, and the average N−Nb−N_{imido} angle is 98.5°. The two

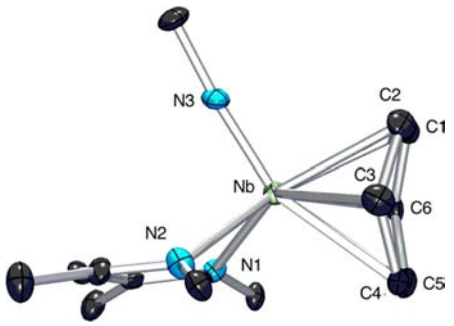

Figure 1. Thermal ellipsoid plot of the complex **2a**. Diisopropyl aryl groups of the BDI ligand have been removed, and ^{t}Bu moieties have been truncated for clarity. Full structure and structural parameters are presented in the SI.

Nb−N_{BDI} distances are 2.246(4) Å, which are similar to those observed in related BDI complexes of Nb(III) and Nb(V).[32,44,46] The Nb−N_{imido}−CMe_3 bond angle (175.3(4)°) is close to linear, and the Nb−N_{imido} distance is 1.775(3) Å, which is also typical of values reported in the literature.[32,44,46] The puckered C_6H_6 ligand of **2a** is characteristic of niobium−arene complexes.[47−50,52,53,57,62] The fold angle at C3···C6 is 22.8°, such that the Nb(1)−C(3) (2.280(5) Å) and Nb(1)−C(6) (2.284(5) Å) distances are shorter than observed for the other four Nb−C bonds (average 2.471(4) Å). These Nb−C distances compare well with Nb−C distances observed previously for arene compounds (from 2.198(5) Å to 2.513(4) Å).[47−62] The C−C bond lengths of the benzene ring vary, with C(1)−C(2) (1.337(6) Å) and C(4)−C(5) (1.384(6) Å) being significantly shorter than bonds involving the C(3) and C(6) atoms (average of 1.450(5) Å).

The ^1H NMR spectrum of the η^6-benzene complex [Nb(BDI)(N^tBu)(η^6-C_6H_6)], **2a**, shows 12 signals, corresponding to a C_s-symmetric Nb(N^tBu)(BDI) moiety, with a singlet (6H) at high-field (3.60 ppm) for the six equivalent benzene protons. The toluene complex [Nb(BDI)(N^tBu)(η^6-Me-C_6H_5)], **2b**, presents similar ^1H NMR spectroscopic features, with three sharp resonances at δ = 3.93, 3.71, 3.59 ppm that were assigned to the aromatic toluene protons and one at δ = 2.0 ppm corresponding to the methyl group of the coordinated toluene. The η^6 aromatic rings of **2a−b** exchange with C_6D_6 (in C_6D_6 solution) within 120 and 20 min, respectively, at room temperature. The ^2H NMR spectrum of **2a-*d*$_6$** also shows a singlet at 3.60 ppm, in accordance with the proposed structure. These ^1H NMR data are consistent with the presence of an averaged η^6-arene adduct in solution (Scheme 1).

Consistent with this behavior, the coordinated arene rings of **2a−b** were found to be readily displaced by carbon monoxide or 2,6-xylyl-isocyanide, leading to the previously reported [Nb(BDI)(N^tBu)$(CO)_2$] (**3**)[44] and [Nb(BDI)(N^tBu)$(CNXyl)_3$] (**4**)[32] complexes, respectively (Scheme 2). Reactivity studies also confirm that the coordinated arene ligands in **2a−b** serve to stabilize the Nb(BDI)(N^tBu) moiety, which can

dx.doi.org/10.1021/ja311966h | J. Am. Chem. Soc. 2013, 135, 3224−3236

Table 1. Selected Bond Distances (in Å) for Complexes 2a, 7a–b, 8, and 9

	2a	7a	7b	8	9
C(1)–C(2)	1.337(6)	1.452(3)	1.462(4)	1.474(3)	1.444(3)
C(2)–C(3)	1.477(7)	1.451(3)	1.476(4)	1.464(3)	1.461(3)
C(3)–C(4)	1.434(7)	1.453(3)	1.422(5)	1.424(4)	1.452(4)
C(4)–C(5)	1.384(6)	1.447(3)	1.451(5)	1.432(4)	1.453(3)
C(5)–C(6)	1.430(8)	1.473(3)	1.443(4)	1.426(3)	1.443(3)
C(6)–C(1)	1.460(6)	1.450(3)	1.475(4)	1.463(3)	1.465(3)
average C–C	1.420	1.454	1.455	1.447	1.453
Nb(1)–C(1)	2.543(5)	2.2599(16)	2.304(4)	2.607(2)	2.301(2)
Nb(1)–C(2)	2.556(5)	2.478(2)	2.296(4)	2.504(2)	2.620(2)
Nb(1)–C(3)	2.280(5)	2.3273(19)	2.630(5)	2.256(2)	2.511(2)
Nb(1)–C(4)	2.385(6)	2.5526(17)	2.518(4)	2.371(2)	2.325(2)
Nb(1)–C(5)	2.400(6)	2.6291(19)	2.324(4)	2.325(2)	2.482(2)
Nb(1)–C(6)	2.284(5)	2.3324(19)	2.446(3)	2.305(2)	2.277(2)
Nb(2)–C(1)	–	2.5533(18)	2.286(4)	2.345(2)	2.605(2)
Nb(2)–C(2)	–	2.3302(19)	2.449(3)	2.202(2)	2.308(2)
Nb(2)–C(3)	–	2.4785(18)	2.328(4)	2.501(2)	2.297(2)
Nb(2)–C(4)	–	2.2673(17)	2.527(5)	2.528(2)	2.460(2)
Nb(2)–C(5)	–	2.324(2)	2.636(4)	2.748(2)	2.294(2)
Nb(2)–C(6)	–	2.6197(19)	2.289(3)	2.835(2)	2.493(2)
Nb(1)–Nb(2)	–	3.914	3.868	3.989	3.876
Nb(1)–Cent	1.956	1.957	1.944	1.919	1.947
Nb(2)–Cent	–	1.959	1.945	2.089	1.932
average Nb(1)–C	–	2.430	2.420	2.395	2.419
average Nb(2)–C	–	2.429	2.419	2.527	2.409
average Nb–C	2.495	2.429	2.419	2.461	2.414
Nb(1)–N(1)	2.245(4)	2.2764(16)	2.249(3)	2.3236(18)	2.289(2)
Nb(1)–N(2)	2.246(4)	2.2136(17)	2.271(3)	2.3109(17)	2.3226(19)
Nb(1)–N(3)	1.775(3)	1.7770(15)	1.776(3)	1.7860(18)	1.774(2)
Nb(2)–N(4)	–	2.2787(16)	2.241(3)	2.2209(18)	2.2983(19)
Nb(2)–N(5)	–	2.2266(15)	2.271(3)	2.2055(18)	2.3287(19)
Nb(2)–N(6)	–	1.7815(15)	1.782(3)	1.7718(19)	1.7819(19)
Nb(1)–N(3)–C(36)	175.3(4)	171.64(15)	175.6(2)	168.65(14)	169.43(19)
Nb(2)–N(6)–C(70)	–	174.83(15)	176.5(3)	174.73(15)	166.62(17)

Scheme 2. Reactivity of Complexes 2a–b

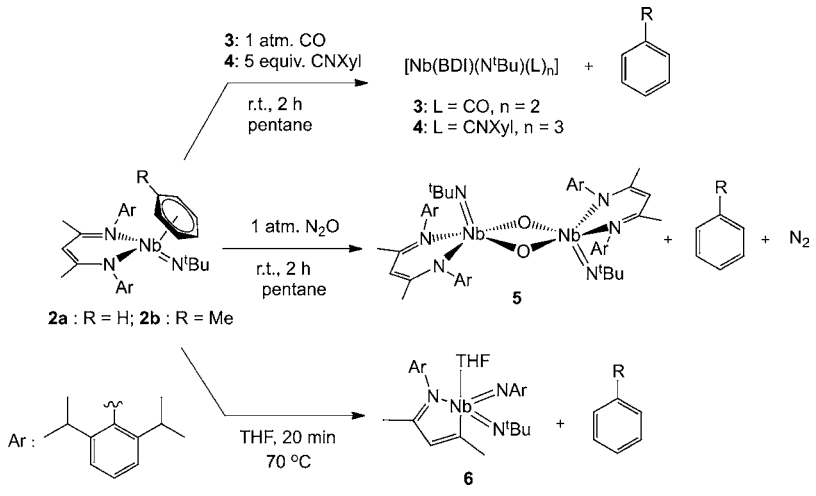

be oxidized by two electrons with suitable substrates. For example, exposure of a benzene solution of **2a** or a toluene solution of **2b** to N_2O (1 atm) quickly leads to the formation of the previously reported μ-oxo dinuclear complex [Nb(BDI)-(N^{t}Bu)(μ-O)]$_2$ (**5**, Scheme 2).[32] In the absence of an external oxidant, loss of the arene via thermolysis of either **2a–b** in THF leads to formation of the bis-imido Nb(V) complex **6** (Scheme 2), where the BDI ligand has been reductively cleaved. This latter compound has been observed previously following hydrogenolysis of **1** in THF, via cleavage of the BDI ligand in the related Nb(III) species [Nb(BDI)(N^{t}Bu)(THF)].[32]

Bimetallic Arene Complexes. *Synthesis.* In an attempt to hinder arene exchange with C_6D_6, ^{1}H NMR spectra of **2a–b** were recorded in C_6D_{12}. Unexpectedly, collecting additional ^{1}H

dx.doi.org/10.1021/ja311966h | J. Am. Chem. Soc. 2013, 135, 3224–3236

Scheme 3. Formation of Complexes 7a−b

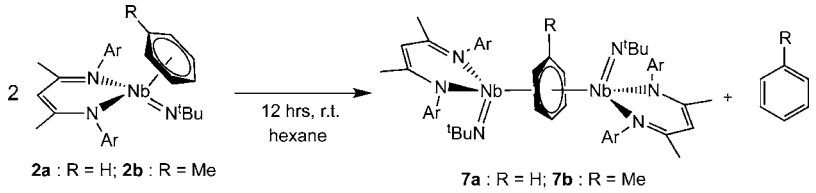

NMR spectra of these solutions after 3 days revealed the clean formation of new diamagnetic arene species that were subsequently formulated as μ-η^6:η^6-arene diniobium inverted sandwich complexes $[[(BDI)Nb(N^tBu)]_2(\mu\eta^6{:}\eta^6\text{-}RC_6H_5)]$ (R = H, **7a** or Me, **7b**; Scheme 3). Red crystals were obtained on a preparative scale in good yields from saturated, dark-red, hexanes solutions of either **2a** or **2b**.

Unlike the monometallic complexes **2a−b** discussed above, and relative to other inverted sandwich molecules reported in the literature,[4,6−8,10−12,14−23] the bridged arenes of **7a−b** did not exchange with deuterated benzene, toluene, or strong π-acidic ligands, such as carbon monoxide or isocyanide, even at temperatures up to 110 °C. To our knowledge, only two other inverted sandwich complexes did not show exchange with solvent molecules at reasonable temperatures.[9,23] Complexes **7a−b** also did not react with small molecules, such as Ph_2N_2, Ph_2S_2, N_2O, organic azides, alkynes, CO_2, and H_2, within a temperature range of 20 to 110 °C, unlike many other inverted sandwich complexes.[4,8,10,14−17,19,23] In contrast, treatment of complex **7a** with either 1 or 2 equiv of $[H(OEt_2][B(C_6F_5)_4]$ produced two products that were formulated as new inverted sandwich complexes, $[[(BDI^{\#})Nb(N^tBu)][(BDI)Nb(N^tBu)](\mu\text{-}\eta^6{:}\eta^6\text{-}C_6H_6)][B(C_6F_5)_4]$ (**8**) and $[[(BDI^{\#})Nb(N^tBu)]_2(\mu\text{-}\eta^6{:}\eta^6\text{-}C_6H_6)][B(C_6F_5)_4]_2$ (**9**) in which one (**8**) or two (**9**) BDI ligands have been protonated (Scheme 4, $BDI^{\#}$ = (ArNC-(Me))$_2$CH$_2$). Compounds **8** and **9** have been synthesized in diethyl ether and chlorobenzene, respectively, and can both be isolated on a preparative scale in good yields. The lack of reactivity at the coordinated benzene ligand may be evidence of a neutral C_6H_6 configuration; however, it is difficult to rule out the possibility that the ancillary ligands are providing steric protection (see Figure S10).

Scheme 4. Formation of Complexes 8 and 9

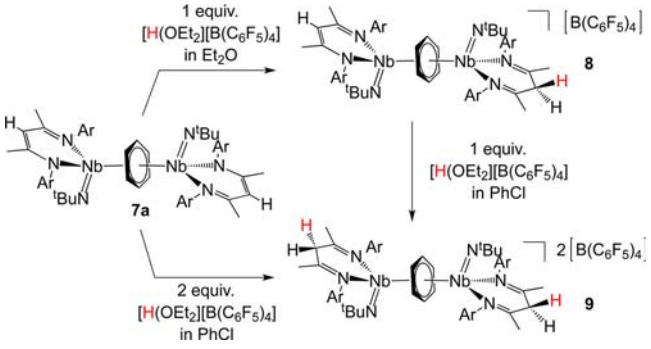

Kinetic Studies. To the best of our knowledge, experimental evidence for the formation of an arene bridged dinuclear complex from a parent, mononuclear species has only been reported once,[23] although related mechanisms have been suggested since the early 1990s.[6] The relatively slow rate of conversion from **2a** to **7a** provides an opportunity to follow the kinetics of this process by ^{1}H NMR spectroscopy. The experiment was performed in C_6D_{12} with 0.07 M **2a** and 4.90 mM internal standard at 334 K. In the absence of benzene, the kinetic data cannot be fitted to a rate law that is either first or second order in **2a** because the concentration of free benzene is changing during the experiments. Introducing an excess of benzene (from 4 to 30 equiv) yields data that are consistent with a dissociative mechanism, and a rate law that is second order in [**2a**] and inverse first order in benzene (Figure 2 and

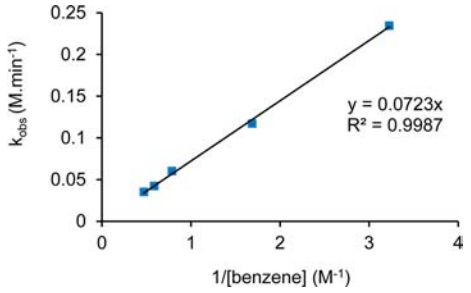

Figure 2. Benzene dependence on the observed second-order rate constant for the formation of **7a**..

Scheme 5. Reactions of the Formation of Complex 7a and Kinetic Law Derivation

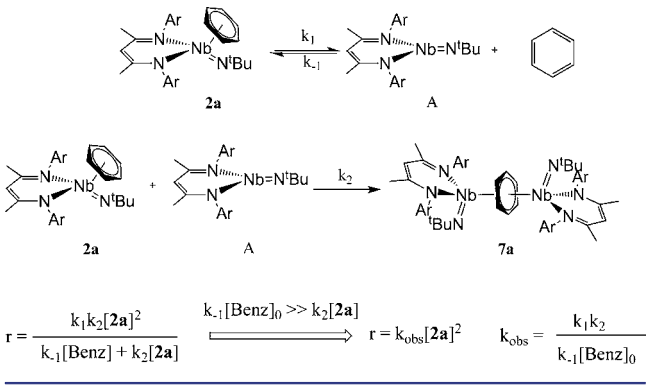

Figure S1). The rate law for the formation of **7a** predicted for the dissociative mechanism illustrated in Scheme 5 is included at the bottom of the graphic. When benzene is in a large excess, the condition k_{-1}[Benz] ≫ k_2[**2a**] is satisfied. Therefore, the formation of complex **7a** follows second-order kinetics, consistent with earlier work,[23] with k_{obs} being inversely proportional to the initial benzene concentration, where k_1k_2/k_{-1} is 0.0723 min^{-1} at 334 K (Figure 2).

Knowing the rate law, an Eyring analysis was performed in the presence of a large excess of benzene (0.593 M, 8 equiv) over the temperature range 313−344 K, at 5 K intervals (Figures 3 and S2). The large enthalpy of activation (28.8(4) kcal·mol^{-1}) is consistent with the slow conversion of **2a−7a** at room temperature. The large positive entropy of activation

dx.doi.org/10.1021/ja311966h | J. Am. Chem. Soc. 2013, 135, 3224−3236

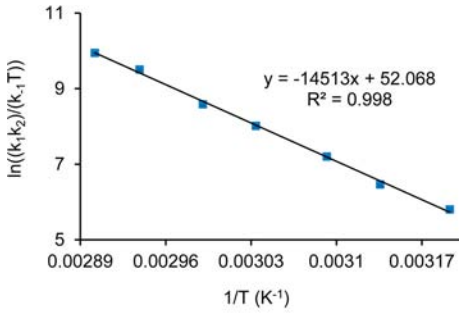

$$(\Delta H_1^{\ddagger} - \Delta H_{-1}^{\ddagger}) + \Delta H_2^{\ddagger} = 28.8\ (4)\ \text{kcal·mol}^{-1}$$

$$(\Delta S_1^{\ddagger} - \Delta S_{-1}^{\ddagger}) + \Delta S_2^{\ddagger} = 56\ (2)\ \text{cal·mol}^{-1}\text{·K}^{-1}$$

Figure 3. Eyring plot for the formation of complex **7a** (top). Activation parameters derived from the Eyring plot (bottom).

(56(2) cal·mol^{-1}·K^{-1}) must be interpreted carefully due to the relatively small temperature range of the study. However, the large positive value further supports a dissociative mechanism in which the first step corresponds to the formation of a three-coordinate species and free benzene (Scheme 5).

X-ray Crystal Structure Descriptions. Thermal ellipsoid plots of complexes **7a**–**b**, **8**, and **9** are shown in Figure 4, and bond distances and angles are summarized in Table 1 (see also the Table S1 for crystallographic parameters). In each of the four inverted sandwich complexes **7a**–**b**, **8**, and **9**, the BDI and imido ligands occupy facial positions in a pseudo-octahedral geometry. Complexes **7a**, **8**, and **9** adopt geometries with dihedral angles between the two imido groups of 114.3°, 132.3°, 117.9° respectively, which minimizes steric repulsion between the aryl rings of the BDI ligands. The BDI-aryls are distorted away from the central toluene ligand in **7b**, resulting in a smaller dihedral angle of 40.6° (Figure 4). Average Nb–N_{BDI} distances are 2.249(2) and 2.258(3) Å in **7a** and **7b**, respectively, and 2.311(2) Å in **9**. Because **8** is dissymmetric, two different sets of average Nb–N_{BDI} distances are observed: 2.317(2) Å on the side with the protonated BDI ligand and 2.203(2) Å on the other.

The C–C distances of the arene rings in **7a**–**b**, **8**, and **9** are all very similar and provide an average C–C distance of 1.45 Å for all four complexes with a standard deviation of 0.02 Å (see Supporting Information, SI). These distances are slightly longer than those reported for free benzene and toluene (1.397(1)[63] and 1.39(1)[64] Å) but in the range of the reported values found for μ-η^6:η^6-arene ligands in the literature.[4−24]

In the four complexes **7a**–**b**, **8** and **9**, the bridging arenes are nonplanar. Observed Nb–C bond distances vary widely for **7a** (2.2673(17)–2.6291(19) Å), **7b** (2.286(4)–2.636(4) Å), and **9** (2.277(2) to 2.620(2) Å). The benzene centroid is nearly equidistant from both niobium atoms in **7a**, **7b**, and **9**, with average Nb-centroid bond distances of 1.958 Å (**7a**), 1.944 Å (**7b**), and 1.939 Å (**9**). For complex **8**, in which one of the BDI ligands is protonated, the benzene ligand lies closer to the Nb bearing the protonated ligand (Nb(1)–C range 2.256(2)–2.607(2) Å; Nb(1)–centroid 1.919 Å) than it does to Nb atom with the unprotonated ligand (Nb(2)–C range 2.202(2)–2.835(2) Å; Nb(2)–centroid 2.089 Å). The Nb(1)–Nb(2) distances decrease by 0.046(5) Å from the C_6H_6 complex **7a** (3.914(2) Å) to C_7H_8 complex **7b** (3.868(4) Å), which could be a consequence of changes in bonding or an increase in steric pressure in **7b**. However, the Nb(1)–Nb(2) distances also decrease by 0.038(2) Å from neutral **7a** (3.914(2) Å) to twice-protonated **9** (3.876(2) Å), which is clearer evidence that protonation disrupts the BDI–Nb interaction and enhances bonding between the arene ligand and Nb atoms.

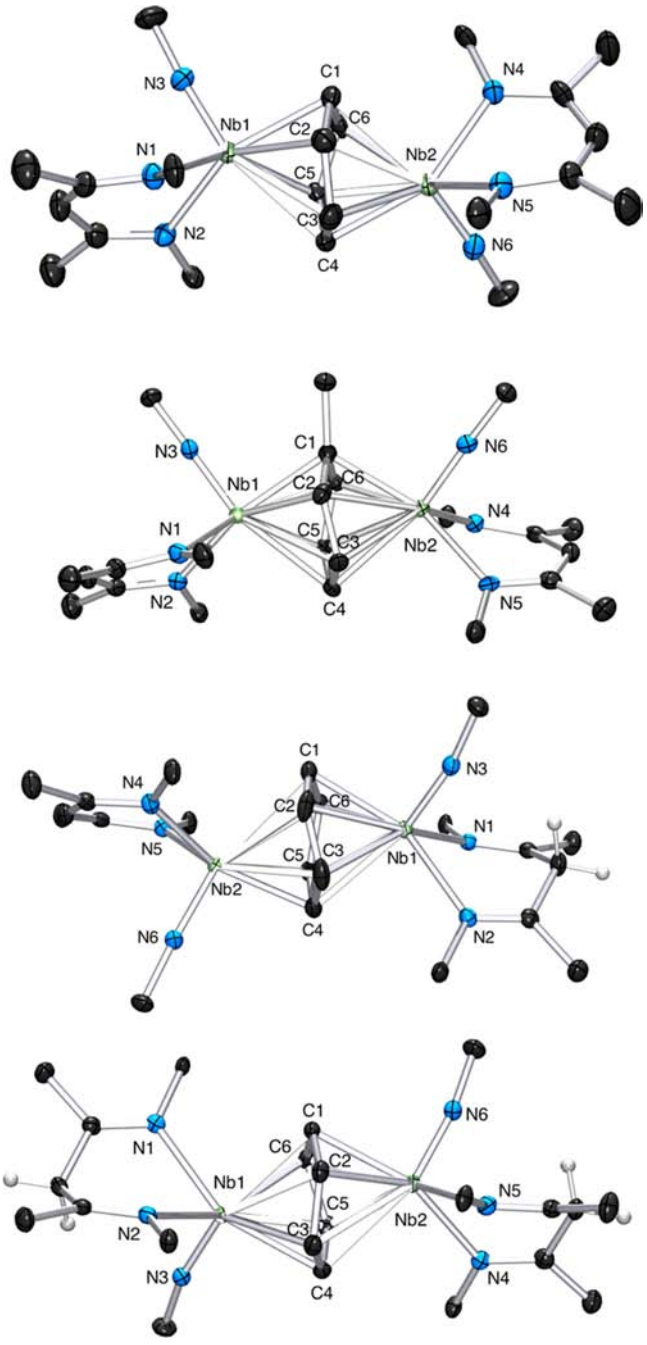

Figure 4. Thermal ellipsoid plots of the complexes **7a** (first), **7b** (second), **8** (third) and **9** (fourth). Diisopropyl aryl groups of the BDI ligand and $B(C_6F_5)_4$ have been removed, and ^{t}Bu moieties have been truncated for clarity. Full structures and structural parameters are presented in the SI.

The mean deviation of the arene rings from planarity is 0.051, 0.052, 0.050, and 0.053 Å respectively, while the largest distortions from the mean plane are 0.170 Å (**7a**), 0.147 Å (**7b**), 0.159 Å (**8**), and 0.163 Å (**9**). The deviation from planarity was also measured from the different dihedral angles of the ring, with average distortions of 14.4° (**7a**), 15.1° (**7b**), 15.2° (**8**), and 15.2° (**9**) (see the SI). Such deformations of the

dx.doi.org/10.1021/ja311966h | J. Am. Chem. Soc. 2013, 135, 3224−3236

η^6,η^6-arene ring have been described in the literature[6,7,9,10,13,16,17,19,20] and support three possible conclusions: (i) the arene ring is significantly reduced, such that there is a disruption of aromaticity and the carbon atoms are best regarded as sp^3 hybridized; (ii) the distortions are sterically induced; or (iii) both these electronic and steric factors are at work. Therefore, additional measurements were performed to understand whether the origin of these structural deformations is inherent to the electronic structure of these complexes.

NMR Spectroscopy. The ^{1}H NMR spectrum of **7a** exhibits one singlet for the methyl groups of both the BDI ligands, one singlet for the equivalent ^{t}Bu groups of the imido ligands, and one singlet (δ = 2.21 ppm) for the benzene ring. These data are consistent with free rotation of the (BDI)Nb(N^{t}Bu) moieties in solution around the Nb···Nb axis, resulting in an average C_{2v} symmetry on the ^{1}H NMR time scale at room temperature (see Scheme 6). Although the spectrum of the benzene complex **7a** remains unchanged down to 213 K in C_7D_8, lowering the temperature to 213 K for the toluene derivative **7b** results in a ^{1}H NMR spectrum that reflects the same C_2-symmetric coordination environment observed in the solid state, thus implying that the dynamic motion has been frozen on the ^{1}H NMR time scale. Variable-temperature ^{1}H NMR data collected between 213 and 383 K provided a coalescence temperature of T_c = 300(2) K (Figure S4). Thermodynamic parameters for this geometrical rearrangement were also measured via a selective inversion recovery (SIR) experiment, yielding $\Delta H^{\ddagger}$= 13.9(6) kcal mol^{-1} and $\Delta S^{\ddagger}$= −4(2) cal K^{-1} mol^{-1} (Figures 5, S6, and S7).

Scheme 6. Proposed Dynamic Processes Observed in Solution for Complex 7b

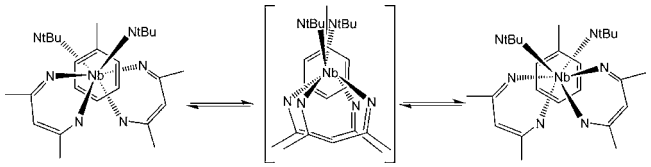

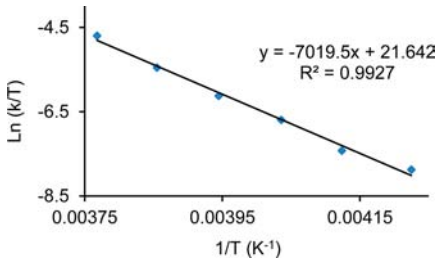

Figure 5. Eyring plots for the dynamic processes observed by ^{1}H NMR in tol-d_8 for complex **7b**.

As expected, the room-temperature ^{1}H NMR spectrum of complex **8** reflects a lower symmetry coordination environment than that in **7a**–**b**, involving two singlets (6H) for the methyl groups of the two different BDI ligands, two singlets (9H) for each of the ^{t}Bu substituents on the two imido groups, and a singlet for the C_6H_6 ligand (δ = 2.40 ppm). Complex **9**, which has two protonated BDI ligands, exhibits two singlets for the methyl groups of the BDI ligands, one singlet for the ^{t}Bu groups and a singlet for the benzene ring (δ = 2.55 ppm). This indicates that the dynamic motion in this complex is slow on the ^{1}H NMR time scale at room temperature. Although **9** undergoes slow decomposition at temperatures higher than 335 K, a variable-temperature experiment (295–330 K) provided a coalescence temperature (T_c = 320(2) K, Figure S5) which was higher than for complex **7b** (T_c = 300(2) K). A SIR experiment was not possible due to the small chemical shift difference of the exchanging peaks. The coalescence temperature trend measured for the geometrical rearrangement of **7a**–**b**, **8**, and **9** (T_c < 213 K, = 300 K, < 230 K, and = 320 K, respectively) is not strictly consistent with what would be expected from steric considerations. Rather, the solution data suggest that the interaction between the arene and the metal centers is stronger in **9** relative to both **7a** and **7b**, resulting in a higher activation barrier of the geometric rearrangement.

The ^{1}H NMR resonances of the bridging arene rings of **7a**–**b**, **8**, and **9** are all found in the 2–3 ppm range, which is consistent with data provided for a diamagnetic, Hf inverted sandwich of toluene (3.12 to 3.34 ppm).[6] The chemical shifts of the benzene rings observed in **7a** (2.21 ppm) were slightly more shielded than those observed for **9** (2.53 ppm). Shifts to higher field from the free arene could result from either sp^3 hybridization of the carbon due to covalent bonding with the metal centers or from a strong shielding effect from the flanking rings on the BDI ligand.

Proton-coupled ^{13}C NMR spectroscopy was performed to determine arene $^1J_{CH}$ values and further refine the bonding models proposed above. The coupling constants were found to be J_{CH} = 178.2(6) Hz for **7a**, J_{CH} = 178.9(7) Hz for complex **8**, and J_{CH} = 184.5(6) Hz for **9**. A similar experiment performed on the monometallic complex **2a** gave a J_{CH} value of 170.5(6) Hz. These differ from the corresponding parameters for aromatic sp^2 carbons (160(1) Hz) by approximately +20 Hz for bimetallic complexes **7a**, **8**, and **9** and by +10 Hz for complex **2a**.[65] Such increases in coupling strength are inconsistent with a decrease in s-character relative to an sp^2-hybridized aromatic carbon and suggest that coordination of the Nb atoms does not result in a formal sp^3 hybridization of the bridging arene-ring atoms. Taken together, the NMR data lead us to conclude that the upfield chemical shifts of the benzene ring are due to shielding induced by the ligand set. This effect has been previously observed in the Nb(BDI)-(N^{t}Bu) system.[44]

As an additional note, the amplitude of the observed coupling constant J_{CH} is also proportional to the electron density located on the atom.[66] Hence, the magnitude of the increase in J_{CH} is due to electron density donated from the niobium metal centers to the arene ligands in **2a**, **7a**, **8**, and **9**. The relative amount of donation may be evaluated by consideration of the J_{CH} coupling constants in a manner related to the accepted practice of using shifts in ν_{CO} as a measure of the metal-based electron density in carbonyl complexes.[67] In the present case, the ^{1}H NMR data indicate that Nb → benzene donation increases in the order **2a** < **7a** ≈ **8** < **9**. These solution data are also correlated with the slight decrease observed in Nb(1)–Nb(2) distances in the solid state for **7a** (3.914(2) Å) relative to **9** (3.876(4) Å).

Optical Spectroscopy. UV–vis spectra were recorded to further investigate the electronic structure of monometallic **2a**–**b** and bimetallic **7a**–**b**, **8**, and **9** (Figure 6 top). Each of the bimetallic complexes has one band at high energy (340–360 nm, 27 700–29 410 cm^{-1}) that gradually decreases in intensity in the order **7a** = **7b** > **8** > **9**. These bands are assigned to intraligand transitions and show a decrease in intensity upon

dx.doi.org/10.1021/ja311966h | J. Am. Chem. Soc. 2013, 135, 3224–3236

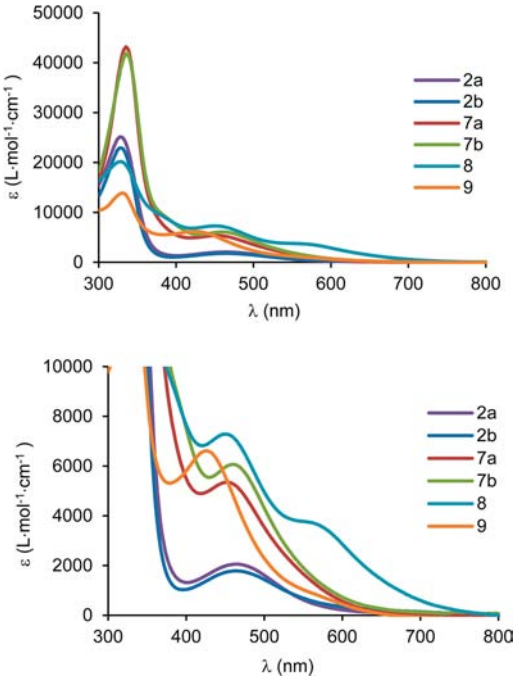

Figure 6. Electronic absorbance spectrum of 87.8 μM solution of **2a** in benzene, 76.0 μM solution of **2b** in toluene, 47.8 μM solution of **7a** in benzene, 56.2 μM solution of **7b** in toluene, 61.3 μM solution of **8**, and 36.4 μM solution of **9** in α,α,α-trifluorotoluene. Full spectrum (top), zoom on the visible area (bottom).

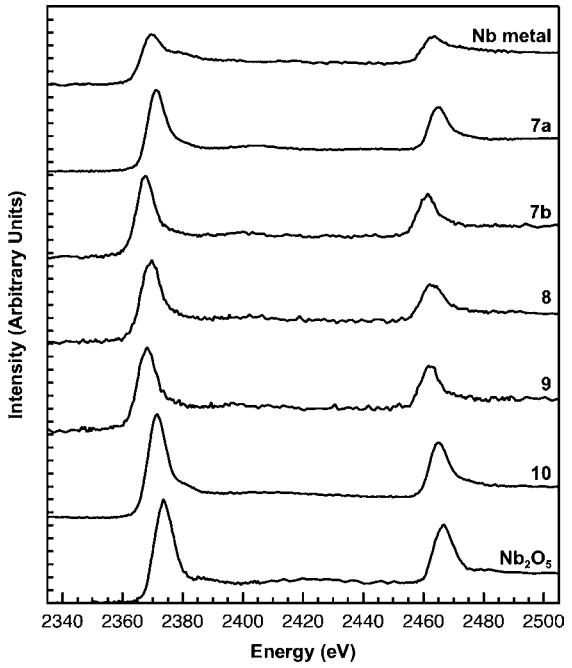

Figure 7. Representative background-subtracted Nb $L_{3,2}$-edge XANES spectra for compounds **7a**–**b**, **8**, and **9**. Also included are reference materials **10**, Nb metal, and Nb_2O_5. All data was collected using a STXM.

protonation of the BDI ligands in **8** and **9**, which disrupts the conjugation of the BDI π-system. The spectra also exhibit broad d–d bands at around 460 nm for **2a**–**b** and **7a**–**b** and 425 nm for **9** (Figure 6 bottom). Complex **8** shows two bands at 460 and 580 nm, which is in agreement with the dissymmetric structure. Spectral intensities (ε) in this region are unusually large for d–d transitions ($\varepsilon \approx 2000$ cm^{-1}·M^{-1} for the monometallic species and $4000 < \varepsilon < 8000$ cm^{-1}·M^{-1} for the bimetallic species). Large values of ε can be explained by a mixture of d- and π-character in the final state orbital that is involved in the transition.[68] These transitions are, therefore, partially Laporte allowed, which results in unusually high intensities for d–d transitions. This concept of metal–arene mixed transitions has been described previously and supports Nb–arene mixing in the inverted sandwich complexes.[21] The absorption spectroscopy data reinforce the bonding picture developed above with the J_{CH} analysis, which suggests that coordination of a second Nb atom to form a bimetallic Nb–arene–Nb interaction enhances Nb–C orbital mixing.

XANES spectroscopy. XANES spectra were obtained using a scanning transmission X-ray microscope (STXM) to evaluate the 4d-electron count of Nb atoms in **7a**–**b**, **8**, and **9** through comparison with reference materials [Nb(BDI)(N^tBu)Cl_2py], **10**; Nb_2O_5 and Nb powder (Figure 7). The 4d-orbital occupancies were determined from normalized Nb $L_{3,2}$-edge intensities, in analogy to measurements made using electron energy-loss spectroscopy (EELS) at the Nb L[69−72] and M-edges.[73−75]

In our experiments, the L-edge absorptions arise from dipole allowed $2p^6 4d^n \rightarrow 2p^5 4d^{n+1}$ transitions that are split by roughly 94 eV into L_3 ($2p_{3,2}$) and L_2 ($2p_{1/2}$) edges due to spin–orbit coupling of the core hole.[76] The intensities of the L_3 and L_2 edges were corrected for the background and normalized by dividing by the continuum intensity, as described previously and in the Experimental Section (Figure 7).[69,70] Integer values for the occupancy of the Nb 4d orbitals were determined assuming a $4d^4 5s^1$ valence electron configuration for Nb metal; however, hybridization may account for some variation in the 4d-orbital occupancies from strictly integer values.[70] The normalized Nb $L_{3,2}$-edge intensities of 0.48(2) and 0.91(4) for Nb metal and Nb_2O_5 reference materials, respectively, agree well with those previously reported by Bach and co-workers and are consistent with an increase in Nb $L_{3,2}$-edge intensity with decreasing 4d-orbital occupancy (Figure 8).[70] As expected, a +5 formal oxidation state for the Nb atom in **10** is determined from the normalized edges intensity of 0.89(5). An increase in Nb 4d-orbital occupancy is reflected by a decrease in the edges intensity to 0.65(3) and 0.68(4) for **7a** and **7b**, respectively. These results suggest that **7a** and **7b** are best described as having neutral arene ligands and Nb atoms with $4d^2$ electronic configurations (+3 formal oxidation states). The same electronic configurations for **8** and **9** were also derived from white-line intensities of 0.69(2) and 0.67(2), respectively. Using these assignments, a plot of the normalized white-line intensity versus 4d-orbital occupancy for **7a**–**b**, **8**, **9**, **10**, Nb powder, and Nb_2O_5 was developed (Figure 8). A linear fit of the data in Figure 8 provides a reliable equation ($I_{4d} = (0.889 \pm 0.012) - (0.107 \pm 0.006) n_{4d}$) and confirms a $4d^2$ configuration for the Nb atoms in **7a**–**b**, **8**, and **9**. Future efforts will be focused on comparisons with related d^1, d^2, and d^3 systems in order to fully assess the extent of mixing between the arene ligand and Nb atoms.

■ CONCLUSIONS

Described here are high-purity syntheses of four diniobium, inverted sandwich compounds, [[(BDI)Nb(N^tBu)]$_2$(μ-RC_6H_5)] (**7a**: R = H and **7b**: R = Me), monocationic **8** [[(BDI$^{\#}$)Nb(N^tBu)][(BDI)Nb(N^tBu)](μ-C_6H_5)]$^{1+}$, and dica-

dx.doi.org/10.1021/ja311966h | J. Am. Chem. Soc. 2013, 135, 3224−3236

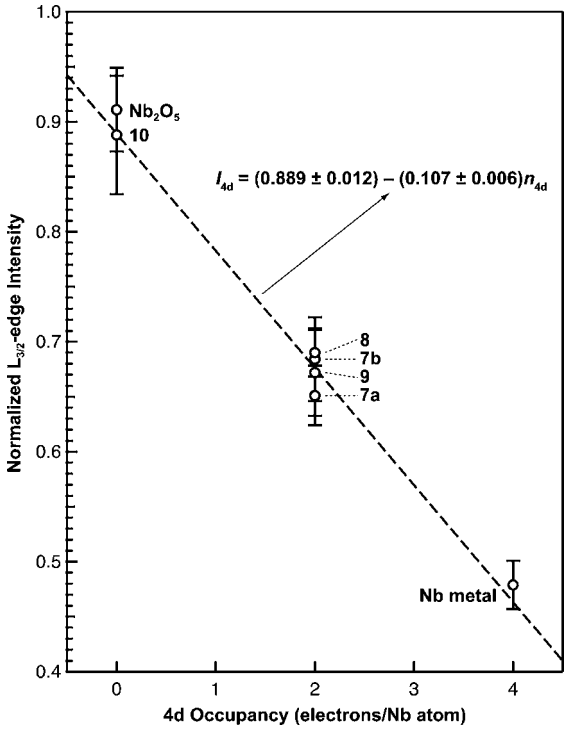

Figure 8. A plot of normalized $L_{3,2}$-edge intensity vs 4d occupancy of **7a–b**, **8**, **9**, **10**, Nb_2O_5, and Nb metal. Error bars are taken from the standard deviation in the intensities determined over repeated measurements. A linear fit to all data (dashed line) gives the equation shown.

tionic **9** $[[(BDI^{\#})Nb(N^tBu)]_2(\mu\text{-}RC_6H_5)]^{2+}$ ($BDI^{\#}$ = $(ArNC(Me))_2CH_2$). Both of the neutral complexes **7a** and **7b** were synthesized directly from their monometallic precursors **2a** and **2b**, which is a new approach to access the chemistry of inverted sandwich compounds. The kinetics of formation of **7a** from **2a** were determined using ^{1}H NMR spectroscopy and suggest that the reaction follows a dissociative mechanism that may involve a transient, three-coordinate "(BDI)Nb=N^{t}Bu" intermediate.

The combined structural, reactivity, and spectroscopic data provide new insight into the nuanced bonding interactions that are involved in bimetallic complexes with bridging arene ligands. X-ray crystal structures reveal bridging arene ligands that are distorted from planarity, with carbon atoms deviating from the average plane by as much as 0.16 Å. However, these distortions cannot be ascribed to a disruption of arene aromaticity resulting from Nb→arene donation because of the undefined role of steric strain, which may also be impacting arene reactivity. The ^{1}H NMR spectra also show increases in the arene $^1J_{CH}$ coupling constants relative to those for the free arene, which is inconsistent with an sp^3 hybridization of the bridging arene C atoms. Taken together with the results from the Nb $L_{3,2}$-edge XANES study, there is little support for a model based on a reduced arene or oxidized Nb atoms. However, the magnitudes of the increase in $^1J_{CH}$ also indicate that some Nb→arene donation is present and increases in the order **2a** < **7a** < **9**, a conclusion that is also reached upon examination of the variable temperature ^{1}H NMR data, UV–vis spectra, and the bridged Nb–Nb distances. The Nb→arene donation is not accompanied by a change in formal oxidation state, which is consistent with earlier reports of inverted sandwich complexes based on d-block metals.[4,6−11] Finally, we conclude that the lack of reactivity at the arene ligands in **7a–b** may be a kinetic effect due to the steric bulk of the BDI ligands. Future work will be focused on efforts to further refine our understanding of electronic structure with computational modeling and will include extensions of this chemistry to a wider range of metal systems and ligand sets.

EXPERIMENTAL SECTION

General Considerations. Unless otherwise noted, all reactions were performed either using standard Schlenk line techniques or in an MBraun inert atmosphere glovebox under an atmosphere of purified nitrogen (<1 ppm O_2/H_2O). Glassware, cannulae, and Celite were stored in an oven at ∼160 °C for at least 12 h prior to use. *n*-Pentane, hexanes, Et_2O, THF, toluene, and benzene were purified by passage through a column of activated alumina, stored over 3 or 4 Å molecular sieves, and degassed prior to use.[77] α,α,α-Trifluorotoluene, dichloroethane, and chlorobenzene were dried over P_2O_5, distilled under reduced pressure, degassed, and stored over 4 Å molecular sieves. Deuterated solvents (C_6D_6, C_7D_8, and C_6D_{12}) were dried over sodium/benzophenone, and C_6D_5Cl was dried over CaH_2. The deuterated solvents were then vacuum transferred to a storage flask and degassed before being stored in the drybox. C_6D_6, C_7D_8, and C_6D_5Cl were stored over activated molecular sieves. BDI,[78] Li(BDI)·Et_2O,[79] (BDI)pyCl_2Nb(N^{t}Bu),[44] and (BDI)$(Me)_2$Nb(N^{t}Bu)[44] were prepared using literature procedures. All other reagents were acquired from commercial sources and used as received. NMR spectra were recorded on Bruker AV-300, AVQ-400, AVB-400, DRX-500, AV-500, and AV-600 spectrometers. Chemical shifts were measured relative to residual solvent peaks, which were assigned relative to an external TMS standard set at 0.00 ppm. ^{1}H and ^{13}C NMR assignments were routinely confirmed by ^{1}H–^{1}H (COSY, NOESY) and ^{1}H–^{13}C (HSQC and HMBC) experiments. Samples for UV–vis NIR spectroscopy were prepared in a Schlenk-adapted quartz cuvette and analyzed on a Varian Cary 50 scanning spectrophotometer. The uncorrected melting points were determined using sealed capillaries prepared under nitrogen on an Optmelt SRS. Elemental analyses were performed at the College of Chemistry Microanalytical Laboratory, University of California, Berkeley. The X-ray structural determinations were performed at CHEXRAY, University of California, Berkeley on Bruker SMART 1000 or SMART APEX diffractometers.

(BDI)Nb(N^{t}Bu)(η^6-C_6H_6) (2a). Benzene (30 mL) was added to a 100-mL Schlenk flask containing (BDI)$(Me)_2$Nb(N^{t}Bu) (0.548 g, 0.90 mmol, 1.0 equiv) at room temperature. The clear yellow solution was degassed with two freeze–pump–thaw cycles. While warming the solution during the second cycle, the headspace of the flask was filled with 1 atm of H_2 (70 mL, 2.8 mmol, 3.0 equiv), and the solution was stirred vigorously. The color of the solution turned to dark red within 5 min. After 12 h, the volatile materials were removed under reduced pressure to yield a red powder. Yield: 530 mg, 93%. X-ray suitable crystals were obtained by rapid crystallization from a mixture of toluene/hexanes (30 mg of **2a** in 0.1 mL of solvent at −40 °C for 6 h). ^{1}H NMR (500 MHz, C_6D_6, 293 K): δ(ppm) 7.10 (t, 2 H, *p*-Ar, $^3J_{HH}$ = 7.6 Hz), 6.97 (d, 2 H, *m*-Ar, $^3J_{HH}$ = 7.2 Hz), 5.13 (s, 1 H, *H*C(C(Me)NAr)$_2$), 4.53 (sept, 2 H, C*H*Me$_2$, $^3J_{HH}$ = 6.6 Hz), 3.71 (s, 6 H, C_6H_6), 2.77 (sept, 2 H, C*H*Me$_2$, $^3J_{HH}$ = 6.9 Hz), 1.73 (s, 6 H, HC(C(*Me*)NAr)$_2$), 1.45 (s, 9 H, ^{t}Bu), 1.37 (d, 6 H, CH*Me*$_2$, $^3J_{HH}$ = 6.9 Hz), 1.05 (d, 6 H, CH*Me*$_2$, $^3J_{HH}$ = 6.6 Hz), 1.04 (d, 6 H, CH*Me*$_2$, $^3J_{HH}$ = 6.6 Hz), 1.00 (m, 6 H, CH*Me*$_2$, $^3J_{HH}$ = 6.9 Hz). ^{13}C{^{1}H} NMR (125.8 MHz, C_6D_6, 293 K) δ(ppm) 168.56 (C, HC(*C*(Me)NAr)$_2$), 153.15 (C, Ar), 143.08 (C, Ar), 141.31 (C, Ar), 125.71 (CH, Ar), 125.63 (CH, Ar), 124.06 (CH, Ar), 105.21 (broad, CH, C_6H_6), 103.56 (CH, HC(C(Me)NAr)$_2$), 33.04 (CH_3, Nb=N^{t}Bu, C_β), 28.46 (CH, *C*HMe$_2$ of C=N*Ar*), 27.39 (CH, *C*HMe$_2$ of C=N*Ar*), 25.92 (CH_3, CH*Me*$_2$ of C=N*Ar*), 25.71 (CH_3, CH*Me*$_2$ of C=N*Ar*), 25.07 (CH_3, CH*Me*$_2$ of C=N*Ar*), 24.79 (CH_3, CH*Me*$_2$ of C=N*Ar*), 24.70 (CH_3, HC(C(*Me*)NAr)$_2$). 13C NMR (100 MHz, C6D6, 293 K) δ(ppm) 105.2 (d, CH, *C*6H6, $^1J_{CH}$ = 170 Hz). ^{1}H NMR (500 MHz, C_6D_{12}, 293 K): δ(ppm) 7.12 (dd, 2 H, *m*-Ar, $^3J_{HH}$ = 7.6 Hz, $^4J_{HH}$ = 1.6 Hz), 7.00 (t, 2 H, *p*-Ar, $^3J_{HH}$ = 7.6 Hz), 6.92 (dd, 2 H, *m*′-Ar, $^3J_{HH}$ = 7.6 Hz,

dx.doi.org/10.1021/ja311966h | J. Am. Chem. Soc. 2013, 135, 3224−3236

$^4J_{HH}$ = 1.6 Hz), 5.16 (s, 1 H, *H*C(C(Me)NAr)$_2$), 4.45 (sept, 2 H, C*H*Me$_2$, $^3J_{HH}$ = 6.8 Hz), 3.61 (s, 6 H, C$_6$*H*$_6$), 2.73 (sept, 2 H, C*H*Me$_2$, $^3J_{HH}$ = 6.8 Hz), 1.77 (s, 6 H, HC(C(*Me*)NAr)$_2$), 1.35 (s, 9 H, ^{t}Bu), 1.26 (d, 6 H, CH*Me*$_2$, $^3J_{HH}$ = 6.4 Hz), 1.03 (d, 6 H, CH*Me*$_2$, $^3J_{HH}$ = 6.8 Hz), 1.00 (d, 6 H, CH*Me*$_2$, $^3J_{HH}$ = 6.4 Hz), 0.98 (m, 6 H, CH*Me*$_2$, $^3J_{HH}$ = 6.8 Hz). Anal. calcd for $C_{39}H_{59}N_3Nb_1$ powders: C, 70.99; H, 8.56; N, 6.37. Found: C, 69.61; H, 8.45; N, 6.33. mp: 85−86 °C (decomp).

(BDI)Nb(N^{t}Bu)(η^6-C$_6$D$_6$) (2a-*d*$_6$). Benzene-*d*$_6$ (10 mL) was added to a 50 mL Schlenk flask containing (BDI)(Me)$_2$Nb(N^{t}Bu) (0.219 g, 0.36 mmol, 1.0 equiv) at room temperature. The clear yellow solution was degassed with two freeze−pump−thaw cycles. While warming the solution during the second cycle, the headspace of the flask was filled with 1 atm of H_2 (40 mL, 1.6 mmol, 4.5 equiv), and the solution was stirred vigorously overnight. The volatile materials were removed under reduced pressure to yield a bright red powder (210 mg, 86% yield). The ^{1}H and ^{13}C NMR spectra were similar to those of complex **2a** with the exception of the resonance assigned to the coordinated benzene. ^{2}H NMR (92 MHz, C$_6$D$_6$, 293 K): δ(ppm) 3.60 (br, s, 6D); ^{13}C NMR (125 MHz, C$_6$D$_6$, 293 K): δ(ppm) 79.96 (t, CD, C$_6$D$_6$, $^1J_{CD}$ = 27.5 Hz). mp: (decomp) 84−85 °C.

(BDI)Nb(N^{t}Bu)(η^6-C$_7$H$_8$) (2b). Toluene (30 mL) was added to a 100 mL Schlenk flask containing (BDI)(Me)$_2$Nb(N^{t}Bu) (0.509 g, 0.83 mmol, 1 equiv) at room temperature. The clear yellow solution was degassed with two freeze−pump−thaw cycles. While warming the solution during the second cycle, the headspace of the flask was filled with 1 atm of H_2 (70 mL, 2.8 mmol, 3 equiv), and the solution was vigorously stirred. The solution rapidly turned dark red within 5 min and was stirred for 12 h at room temperature. The volatile materials were removed under reduced pressure to yield a red powder (620 mg, 91%). ^{1}H NMR (500 MHz, C$_7$D$_8$, 293 K): δ(ppm): 7.19 (dd, 2 H, *m*-Ar, $^3J_{HH}$ = 8.0 Hz, $^3J_{HH}$ = 2.0 Hz), 7.09 (t, 2 H, *p*-Ar, $^3J_{HH}$ = 7.6 Hz), 6.97 (dd, 2 H, *m*′-Ar, $^3J_{HH}$ = 7.6 Hz, $^4J_{HH}$ = 1.2 Hz), 5.07 (s, 1 H, *H*C(C(Me)NAr)$_2$), 4.61 (sept, 2 H, C*H*Me$_2$, $^3J_{HH}$ = 6.5 Hz), 3.93 (t, 1 H, *p*-C$_7$H$_8$, $^3J_{HH}$ = 7.5 Hz), 3.71 (t, 2 H, *m*-C$_7$H$_8$, $^3J_{HH}$ = 7.2 Hz), 3.59 (d, 2 H, *o*-C$_7$H$_8$, $^3J_{HH}$ = 5.0 Hz), 2.74 (sept, 2 H, C*H*Me$_2$, $^3J_{HH}$ = 7.0 Hz), 1.70 (s, 6 H, HC(C(*Me*)NAr)$_2$), 1.45 (s, 9 H, ^{t}Bu), 1.37 (d, 6 H, CH*Me*$_2$, $^3J_{HH}$ = 6.6 Hz), 1.15 (d, 6 H, CH*Me*$_2$, $^3J_{HH}$ = 6.0 Hz), 1.40 (s, 3 H, C*H*$_3$ of C$_7$H$_8$), 1.02 (d, 12 H, CH*Me*$_2$, $^3J_{HH}$ = 6.6 Hz). ^{13}C{^{1}H} NMR (125.8 MHz, C$_7$D$_8$, 293 K) δ(ppm) 166.6 (C, HC(*C*(Me)NAr)$_2$), 152.3 (C, Ar), 143.9 (C, Ar), 141.1 (C, Ar), 124.7 (CH, Ar), 124.6 (CH, Ar), 124.0 (CH, Ar), 102 (broad, CH, *C*$_7$H$_8$), 101.5 (CH, *H*C(C(Me)NAr)$_2$), 33.4 (CH$_3$, Nb=N^{t}Bu, C$_\beta$), 29.4 (CH, *C*HMe$_2$ of C=N*Ar*), 27.2 (CH, *C*HMe$_2$ of C=N*Ar*), 26.4 (CH$_3$, CH*Me*$_2$ of C=N*Ar*), 25.9 (CH$_3$, CH*Me*$_2$ of C=N*Ar*), 25.4 (CH$_3$, CH*Me*$_2$ of C=N*Ar*), 24.8 (CH$_3$, CH*Me*$_2$ of C=N*Ar*), 24.50 (CH$_3$, HC(C(*Me*)NAr)$_2$), 23.2 (broad, CH$_3$, *C*$_7$H$_8$). ^{1}H NMR (500 MHz, C$_6$D$_{12}$, 293 K): δ(ppm) 7.14 (dd, 2 H, *m*-Ar, $^3J_{HH}$ = 7.5 Hz, $^4J_{HH}$ = 1.8 Hz), 7.01 (t, 2 H, *p*-Ar, $^3J_{HH}$ = 7.5 Hz), 6.93 (dd, 2 H, *m*′-Ar, $^3J_{HH}$ = 7.8 Hz, $^4J_{HH}$ = 1.5 Hz), 5.12 (s, 1 H, *H*C(C(Me)NAr)$_2$), 4.54 (sept, 2 H, C*H*Me$_2$, $^3J_{HH}$ = 6.6 Hz), 3.81 (q, 1 H, *p*-C$_7$H$_8$, $^3J_{HH}$ = 4.5 Hz), 3.59 (d, 4 H, *o*,*m*-C$_7$H$_8$, $^3J_{HH}$ = 4.5 Hz), 2.70 (sept, 2 H, C*H*Me$_2$, $^3J_{HH}$ = 6.9 Hz), 1.88 (s, 6 H, HC(C(*Me*)NAr)$_2$), 1.37 (s, 9 H, ^{t}Bu), 1.29 (d, 6 H, CH*Me*$_2$, $^3J_{HH}$ = 6.9 Hz), 1.26 (s, 3 H, C*H*$_3$ of C$_7$H$_8$), 1.12 (d, 6 H, CH*Me*$_2$, $^3J_{HH}$ = 6.6 Hz), 1.04 (d, 6 H, CH*Me*$_2$, $^3J_{HH}$ = 6.9 Hz), 1.00 (m, 6 H, CH*Me*$_2$, $^3J_{HH}$ = 6.6 Hz). Anal. calcd for $C_{40}H_{61}N_3Nb_1$ powders: C, 71.30; H, 8.68; N, 6.24. Found: C, 69.59; H, 8.33; N, 6.18. mp: (decomp) 92−93 °C.

[(BDI)Nb(N^{t}Bu)]$_2$(μ-η^6:η^6-C$_6$H$_6$) (7a). Hexanes (50 mL) was added to a 100 mL Schlenk flask containing **2a** (0.378 g, 0.575 mmol). The dark-red solution was stirred for 12 h. The volatile materials were removed under reduced pressure to yield a red powder, which was dissolved in pentane and concentrated to ∼10 mL. The solution was stored at −40 °C, and the bright-red crystals that formed within 1 day were filtered, and residual solvent was removed under reduced pressure. One molecule of pentane remained present in the crystal lattice, as confirmed by elemental analysis and ^{1}H NMR spectroscopy. X-ray suitable crystals were obtained by recrystallization from Et$_2$O. Yield: 0.305 g, 80%. ^{1}H NMR (500 MHz, C$_6$D$_6$, 293 K): δ(ppm) 7.10 (t, 4 H, *p*-Ar, $^3J_{HH}$ = 7.6 Hz), 6.97 (dd, 4 H, *m*-Ar, $^3J_{HH}$ = 7.6 Hz, $^4J_{HH}$ = 1.6 Hz), 4.92 (s, 2 H, *H*C(C(Me)NAr)$_2$), 4.13 (sept, 4 H, C*H*Me$_2$, $^3J_{HH}$ = 6.8 Hz), 3.05 (sept, 4 H, C*H*Me$_2$, $^3J_{HH}$ = 6.8 Hz), 2.41 (s, 6 H, C$_6$*H*$_6$), 1.68 (s, 12 H, HC(C(*Me*)NAr)$_2$), 1.27 (d, 12 H, CH*Me*$_2$, $^3J_{HH}$ = 8.0 Hz), 1.26 (s, 18 H, ^{t}Bu), 1.23 (m, 6H, pentane), 1.153 (d, 12 H, CH*Me*$_2$, $^3J_{HH}$ = 6.4 Hz), 1.145 (d, 12 H, CH*Me*$_2$, $^3J_{HH}$ = 6.8 Hz), 1.08 (d, 12 H, CH*Me*$_2$, $^3J_{HH}$ = 6.8 Hz), 0.83 (t, 6H, pentane). ^{13}C{^{1}H} NMR (125.8 MHz, C$_6$D$_6$, 293 K) δ(ppm) 168.37 (C, HC(*C*(Me)NAr)$_2$), 151.77 (C, Ar), 142.53 (C, Ar), 142.05 (C, Ar), 125.96 (CH, Ar), 125.47 (CH, Ar), 123.93 (CH, Ar), 101.59 (CH, HC(C(Me)NAr)$_2$), 79.96 (CH, *C*$_6$H$_6$), 34.45 (pentane), 32.82 (CH$_3$, Nb=N^{t}Bu, C$_\beta$), 28.94 (CH, *C*HMe$_2$ of C=N*Ar*), 27.21 (CH, *C*HMe$_2$ of C=N*Ar*), 25.95 (CH$_3$, CH*Me*$_2$ of C=N*Ar*), 25.86 (CH$_3$, CH*Me*$_2$ of C=N*Ar*), 25.73 (CH$_3$, CH*Me*$_2$ of C=N*Ar*), 25.70 (CH$_3$, CH*Me*$_2$ of C=N*Ar*), 25.06 (CH$_3$, HC(C(*Me*)NAr)$_2$), 22.72 (pentane), 14.25 (pentane). ^{13}C NMR (125.8 MHz, C$_6$D$_6$, 293 K) δ(ppm) 79.96 (d, CH, *C*$_6$H$_6$, $^1J_{CH}$ = 178.2 Hz). ^{1}H NMR (500 MHz, C$_6$D$_{12}$, 293 K): δ(ppm) 7.04 (dd, 4 H, *m*-Ar, $^3J_{HH}$ = 7.6 Hz, $^4J_{HH}$ = 1.6 Hz), 6.97 (t, 4 H, *p*-Ar, $^3J_{HH}$ = 7.6 Hz), 6.84 (dd, 4 H, *m*′-Ar, $^3J_{HH}$ = 7.6 Hz, $^4J_{HH}$ = 1.6 Hz), 4.93 (s, 2 H, *H*C(C(Me)NAr)$_2$), 3.98 (sept, 4 H, C*H*Me$_2$, $^3J_{HH}$ = 6.8 Hz), 2.91 (sept, 4 H, C*H*Me$_2$, $^3J_{HH}$ = 6.8 Hz), 2.27 (s, 6 H, C$_6$*H*$_6$), 1.69 (s, 12 H, HC(C(*Me*)NAr)$_2$), 1.13 (d, 12 H, CH*Me*$_2$, $^3J_{HH}$ = 6.8 Hz), 1.06 (s, 18 H, ^{t}Bu), 0.995 (d, 12 H, CH*Me*$_2$, $^3J_{HH}$ = 7.2 Hz), 0.96 (d, 12 H, CH*Me*$_2$, $^3J_{HH}$ = 7.4 Hz), 0.94 (d, 12 H, CH*Me*$_2$, $^3J_{HH}$ = 7.5 Hz). Anal. calcd for $C_{77}H_{118}N_6Nb_2$: C, 70.41; H, 9.05; N, 6.40. Found: C, 70.33; H, 9.11; N, 6.51. mp: 117.9−119.4 °C.

[(BDI)Nb(N^{t}Bu)]$_2$(μ-η^6:η^6-C$_6$D$_6$) (7a-*d*$_6$). The complex **2a**-*d*$_6$ (57.1 mg, 0.086 mmol) was stirred in hexanes (20 mL) for 12 h. The dark-red solution was then concentrated to ca. 10 mL and stored at −40 °C to form bright red crystals which were filtered and residual solvent was removed under reduced pressure (43.2 mg, 76% yield). The ^{1}H and ^{13}C NMR spectra were similar to those of complex **2**. ^{2}H NMR (92 MHz, C$_6$D$_6$, 293 K): δ(ppm) 2.2 (br, s, 6D); ^{13}C NMR (125 MHz, C$_6$D$_6$, 293 K): δ(ppm) 79.96 (t, CD, C$_6$D$_6$, $^1J_{CD}$ = 27.45 Hz).

[(BDI)Nb(N^{t}Bu)]$_2$(μ-η^6:η^6-C$_7$H$_8$) (7b). Hexanes (20 mL) was added to a 50 mL flask containing the complex (**2**) (0.104 g, 0.11 mmol). The red solution was stirred overnight, and the volatile materials were removed under reduced pressure to yield a dark-red powder, which was recrystallized from hexanes at −40 °C (10 mL), yielding red crystals that were collected by filtration, and residual solvent was removed under reduced pressure (0.057 mg, 72%). One molecule of pentane remained present in the lattice of the crystal, as confirmed by elemental analysis and ^{1}H NMR spectroscopy. Recrystallization from toluene at −40 °C yielded X-ray suitable crystals within 2 days. ^{1}H NMR (500 MHz, C$_7$D$_8$, 293 K): δ(ppm) 7.10 (broad, Ar + C$_7$D$_8$), 6.90 (dd, 4 H, *m*-Ar, $^3J_{HH}$ = 6.4 Hz, $^4J_{HH}$ = 2.4 Hz), 4.84 (s, 2 H, *H*C(C(Me)NAr)$_2$), 4.5 (broad, 4 H, C*H*Me$_2$, $^3J_{HH}$ = 7.0 Hz), 2.88 (broad, 2 H, *o*-C$_7$H$_8$), 2.83 (broad, 1 H, *p*-C$_7$H$_8$,), 2.76 (broad, 6 H, *m*-C$_7$H$_8$ and C*H*Me$_2$), 1.50 (broad, 12 H, HC(C(*Me*)NAr)$_2$), 1.41 (s, 18 H, ^{t}Bu), 1.31 (d, 12 H, CH*Me*$_2$, $^3J_{HH}$ = 6.4 Hz), 1.14 (d, 6 H, CH*Me*$_2$, $^3J_{HH}$ = 6.8 Hz), 1.04 (d, 18 H, CH*Me*$_2$, $^3J_{HH}$ = 7.0 Hz), 0.61 (broad, 6 H, CH*Me*$_2$), 0.40 (broad, 6 H, CH*Me*$_2$). (500 MHz, C$_7$D$_8$, 353 K): δ(ppm) 7.10 (broad, Ar + C$_7$D$_8$), 6.90 (d, 4 H, *m*-Ar, $^3J_{HH}$ = 7.6 Hz), 4.86 (s, 2 H, *H*C(C(Me)NAr)$_2$), 4.39 (sept, 4 H, C*H*Me$_2$, $^3J_{HH}$ = 7.0 Hz), 2.88 (broad, 2 H, *o*-C$_7$H$_8$), 2.83 (broad, 1 H, *p*-C$_7$H$_8$,), 2.76 (broad, 6 H, *o*-C$_7$H$_8$ and C*H*Me$_2$), 2.04 (s, 3 H, C*H*$_3$ of C$_7$H$_8$), 1.53 (s, 12 H, HC(C(*Me*)NAr)$_2$), 1.38 (s, 18 H, ^{t}Bu), 1.20 (d, 12 H, CH*Me*$_2$, $^3J_{HH}$ = 6.5 Hz), 1.07 (d, 12 H, CH*Me*$_2$, $^3J_{HH}$ = 7.0 Hz), 1.05 (broad, 12 H, CH*Me*$_2$), 0.77 (broad, 12 H, CH*Me*$_2$). ^{13}C{^{1}H} NMR (125.8 MHz, C$_7$D$_8$, 353 K) δ(ppm) 167.95 (C, HC(*C*(Me)NAr)$_2$), 151.66 (C, Ar), 143.23 (C, Ar), 126.25 (CH, Ar), 124.42 (CH, Ar), 102.98 (CH, HC(C(Me)NAr)$_2$), 87.53 (CH, *C*$_7$H$_8$), 43.06 (CH$_3$, *C*$_7$H$_8$), 32.90 (CH$_3$, Nb=N^{t}Bu, C$_\beta$), 28.29 (CH, *C*HMe$_2$ of C=N*Ar*), 27.43 (CH, *C*HMe$_2$ of C=N*Ar*), 25.95 (CH$_3$, CH*Me*$_2$ of C=N*Ar*), 26.52 (CH$_3$, CH*Me*$_2$ of C=N*Ar*), 25.73 (CH$_3$, CH*Me*$_2$ of C=N*Ar*), 25.54 (CH$_3$, CH*Me*$_2$ of C=N*Ar*), 25.29 (CH$_3$, HC(C(*Me*)NAr)$_2$). Anal. calcd for $C_{78}H_{120}N_6Nb_2$: C, 70.57; H, 9.11; N, 6.33. Found: C, 70.24; H, 9.85; N, 6.20. mp: 132.1−133.7 °C.

Formation of [(BDI)Nb(N^{t}Bu)(L)$_x$] (3: L = CO, *x* = 2 and 4: L = XylNC, *x* = 3). CO (1 atm) was added to an evacuated J-Young tube containing **2a** (12.0 mg, 18.2 mmol) or **2b** (17.2 mg, 25.7 mmol) in

C_6D_{12}, resulting in a slow color change from dark red to green within 6 or 4 h, respectively. Solution analysis by ^1H and ^{13}C NMR spectroscopies agreed with the formation of the previously reported complex **3** (BDI)Nb(N^tBu)$(CO)_2$.[44] Similarly, 5 equiv of XylNC (10.9 mg, 83.1 mmol) were added to a J-Young tube containing **2a** (11.2 mg, 17.8 mmol) or **2b** (13.5 mg, 20.0 mmol) in C_6D_{12}, resulting in a fast color change from dark red to purple within 2 h or 40 min, respectively. The product formed was assigned by ^1H and ^{13}C NMR spectroscopies to the previously reported complex **4** (BDI)Nb(N^tBu)$(CNXyl)_3$.[32]

Reaction with N_2O to Form [(BDI)Nb(N^tBu)(μ_2-O)]$_2$ (5). Addition of 1 atm of N_2O to a J-Young tube containing **2a** (11.8 mg, 17.2 mmol) in C_6D_6 or **2b** (13.2 mg, 19.6 mmol) in C_7D_8 resulted in a color change from dark red to bright orange within 20 or 5 min, respectively with yellow microcrystalline material rapidly crystallizing out of the solution. This yellow material has been assigned by ^1H NMR spectroscopy in both cases to the previously synthesized [(BDI)Nb(N^tBu)(μ_2-O)]$_2$ complex **4**.[32]

Formation of (N(Ar)C(CH_3)CHC(CH_3))(THF)Nb(N^tBu)(NAr) (6). Heating a solution of **2a** (11.2 mg, 17.0 mmol) or **2b** (11.9 mg, 17.8 mmol) in THF-d_8 to 70 °C for 1 h resulted in the formation of **6** (confirmed by ^1H NMR spectroscopy), which was previously synthesized via a different route.[32]

[[(BDI$^{\#}$)Nb(N^tBu)][(BDI)Nb(N^tBu)](μ-η^6:η^6-C_6H_6)][B(C_6F_5)$_4$] (8). Et_2O (20 mL) was added to a 50 mL flask containing the complex [(BDI)Nb(N^tBu)]$_2$(μ-η^6:η^6-C_6H_6) (**7a**) (0.180 g, 0.136 mmol, 1.0 equiv), and the red solution was cooled to −80 °C. Ten mL of a diethylether solution of [(H(OEt_2)][B(C_6F_5)$_4$] (97 mg, 0.143 mmol, 1.05 equiv) was added to the red solution, and the mixture was stirred at −80 °C for 20 min, warmed to room temperature and stirred overnight. The purple microcrystalline material that formed was separated by filtration, washed with Et_2O (2 × 20 mL) and extracted with DCE (10 mL). The resulting purple solution was cooled at −15 °C to yield dark purple crystals (150 mg, 61%). X-ray suitable crystals were obtained by recrystallization from DCE. ^1H NMR (500 MHz, C_6D_5Cl, 293 K): δ (ppm) 7.16−6.87 (multiple peaks, broad, Ar + C_6D_5Cl), 5.05 (s, 1 H, *H*C(C(Me)NAr)$_2$), 4.99 (d, 1 H, C*H*H′(C-(Me)NAr)$_2$), $^2J_{HH}$ = 16.3 Hz), 3.79 (d, 1 H, CH*H*′(C(Me)NAr)$_2$), $^2J_{HH}$ = 16.2 Hz), 3.70 (sept, 2 H, C*H*Me$_2$, $^3J_{HH}$ = 7.0 Hz), 3.47 (sept, 2 H, C*H*Me$_2$, $^3J_{HH}$ = 7.0 Hz), 2.75 (sept, 2 H, C*H*Me$_2$, $^3J_{HH}$ = 7.0 Hz), 2.40 (s, 6 H, C_6H_6), 1.90 (sept, 2 H, C*H*Me$_2$, $^3J_{HH}$ = 7.0 Hz), 1.80 (s, 6 H, CHH′(C(*Me*)NAr)$_2$), 1.63 (s, 6 H, CH(C(*Me*)NAr)$_2$), 1.12 (d, 6 H, CH*Me*$_2$, $^3J_{HH}$ = 6.8 Hz), 1.08 (s, 9 H, ^{t}Bu), 1.01 (d, 6 H, CH*Me*$_2$, $^3J_{HH}$ = 6.4 Hz), 1.00 (d, 6 H, CH*Me*$_2$, $^3J_{HH}$ = 6.8 Hz), 0.95 (d, 6 H, CH*Me*$_2$, $^3J_{HH}$ = 7.0 Hz), 0.92 (d, 6 H, CH*Me*$_2$, $^3J_{HH}$ = 6.4 Hz), 0.88 (d, 6 H, CH*Me*$_2$, $^3J_{HH}$ = 6.4 Hz), 0.85 (d, 6 H, CH*Me*$_2$, $^3J_{HH}$ = 6.4 Hz), 0.84 (s, 9 H, ^{t}Bu), 0.74 (d, 6 H, CH*Me*$_2$, $^3J_{HH}$ = 6.4 Hz). $^{13}C\{^1H\}$ NMR (125.8 MHz, C_6D_5Cl, 293 K) δ(ppm) 167.5 (C, HC(*C*(Me)-NAr)$_2$), 164.9 (C, HC(*C*(Me)NAr)$_2$), 151.66 (C, Ar), 150.5 (C, Ar), 147.3 (C, Ar), 143.23 (C, Ar), 140.03 (CH, Ar), 138.5 (CH, Ar), 126.25 (CH, Ar), 124.42 (CH, Ar), 102.98 (CH, HC(C(Me)NAr)$_2$), 80.6 (CH, C_6H_6), 68.8 (CH_2, H_2C(C(Me)NAr)$_2$), 32.9 (CH_3, Nb═N^{t}Bu, C_β), 31.4 (CH_3, Nb═N^{t}Bu, C_β), 29−27 (CH, *C*HMe$_2$ of C═N*Ar*), 25−22 (CH_3, CH*Me*$_2$ of C═N*Ar*). ^{13}C NMR (125.8 MHz, C_6D_5Cl, 293 K) δ(ppm) 80.6 (d, CH, C_6H_6, $^1J_{CH}$ = 178.9 Hz). ^{19}F NMR (470.4 MHz, C_6D_5Cl, 293 K) δ(ppm) −133.8, −166.1, and −169.6 (B(C_6F_5)$_4$). Anal. calcd for $C_{96}H_{107}N_6Nb_2B_1F_{20}$: C, 60.01; H, 5.61; N, 4.37. Found: C, 59.76; H, 5.56; N, 4.30. mp: 215.4−217.5 °C.

[[(BDI$^{\#}$)Nb(N^tBu)]$_2$(μ-η^6:η^6-C_6H_6)][B(C_6F_5)$_4$]$_2$ (9). Chlorobenzene (20 mL) was added to a 50 mL flask containing the complex [[(BDI$^{\#}$)Nb(N^tBu)][(BDI)Nb(N^tBu)](μ-η^6:η^6-C_6H_6)][B(C_6F_5)$_4$] (**8**) (0.180 g, 0.09 mmol, 1 equiv). To the dark-purple solution was added 10 mL a chlorobenzene solution of [(H(OEt_2)][B(C_6F_5)$_4$] (168 mg, 0.20 mmol, 2.1 equiv) at room temperature, and the mixture was stirred overnight, resulting in a clear orange solution. The volatile materials were removed under reduced pressure to yield an orange powder, which was washed with Et_2O (2 × 20 mL) and extracted with 10 mL α,α,α-trifluorotoluene. Et_2O (20 mL) was layered over the α,α,α-trifluorotoluene solution at room temperature, yielding bright-orange X-ray suitable crystals within 2 days, which were filtered, and residual solvent was removed under reduced pressure (100 mg, 42%). One molecule of α,α,α-trifluorotoluene remained present in the lattice of the crystal, as confirmed by elemental analysis, X-ray crystallography, and ^1H NMR spectroscopy. ^1H NMR (500 MHz, C_6D_5Cl, 293 K): δ (ppm) 7.38 (broad, 2 H, Ar), 7.20 (broad, 4 H, Ar), 7.06 (broad, 2 H, Ar), 6.90 (broad, 2 H, Ar), 6.84 (broad, 2 H, Ar), 4.78 (d, 1 H, C*H*H′(C(Me)NAr)$_2$), $^2J_{HH}$ = 16.5 Hz), 3.98 (d, 1 H, CH*H*′(C(Me)-NAr)$_2$), $^2J_{HH}$ = 16.2 Hz), 3.30 (broad, 2 H, C*H*Me$_2$), 3.14 (broad, 2 H, C*H*Me$_2$), 2.55 (s, 6 H, C_6H_6), 1.90 (s, 6 H, CHH′(C(*Me*)NAr)$_2$), 1.83 (broad, 10 H, CH(C(*Me*)NAr)$_2$ + 2 C*H*Me$_2$), 1.08 (broad, 12 H, CH*Me*$_2$), 0.94 (broad, 12 H, CH*Me*$_2$), 0.84 (s, 30 H, ^{t}Bu), 0.73 (broad, 12 H, CH*Me*$_2$). $^{13}C\{^1H\}$ NMR (125.8 MHz, C_6D_5Cl, 293 K) δ(ppm) 167.95 (C, H_2C(*C*(Me)NAr)$_2$), 150.5 (C, Ar), 147.3 (C, Ar), 140.03 (CH, Ar), 138.5 (CH, Ar), 84.16 (CH, C_6H_6), 68.8 (CH_2, H_2C(C(Me)NAr)$_2$), 31.4 (CH_3, Nb═N^{t}Bu, C_β), 29−27 (CH, *C*HMe$_2$ of C═N*Ar*), 25−22 (CH_3, CH*Me*$_2$ of C═N*Ar*). ^{13}C NMR (125.8 MHz, C_6D_5Cl, 293 K) δ(ppm) 84.2 (d, CH, C_6H_6, $^1J_{CH}$ = 184.5 Hz). ^{19}F NMR (470.4 MHz, C_6D_5Cl, 293 K) δ(ppm) −62.7 ($PhCF_3$), −133.8, −166.1, and −169.6 (B(C_6F_5)$_4$). Anal. calcd for $C_{131}H_{120}B_2F_{43}N_6Nb_2$: C, 56.50; H, 3.69; N, 3.02. Found: C, 56.63; H, 3.81; N, 2.78. mp: 204.9−206.2 °C.

Kinetic Studies. The kinetics of the reaction that transformed **2a** to **7a** were followed by ^1H NMR spectroscopy in a J-Young tube with a 0.07 M solution of **2a** in C_6D_{12} at different temperatures and in presence of various concentrations of benzene. The rate constants determined by the disappearance of starting material and appearance of product were identical. The mass balance was conserved through the course of each experiment. When the C_6D_{12} was stored over molecular sieves, the kinetics data were inconsistent and not reproducible. This was attributed to the acidity of the sieves,[80] which may lead to the formation of side products. Reproducible kinetic data were obtained either by using NMR solvents stored in the absence of molecular sieves or by stirring the solvent over basic alumina and filtering prior to use. Complex **2a** was added to a J-Young tube (22.1−23.3 mg, 0.032−0.033 mmol), followed by 0.4 mL of C_6H_6/C_6D_{12} stock solution containing 4.92 mM internal standard (tetrakis(trimethylsilyl)silane). The concentration of each species was calculated by integrating the methyl peaks of the BDI backbone (1.77 ppm for complex **2a** and 1.69 ppm for complex **7a**) relative to the internal standard. All data used for the Eyring plot were obtained using the same C_6D_{12}-C_6H_6-internal standard stock solution to minimize experimental error (4.92 mM internal standard and 0.593 M C_6H_6). Temperatures inside the probe were determined as a function of the frequency difference (in Hz) between the two signals observed for a sample containing 100% ethylene glycol.[81]

SIR Experiments.[82,83] The kinetics of the intramolecular rearrangement reactions was studied at six different temperatures within the range of 235−265 K. Temperatures were calculated using a 100% methanol sample by measuring the separation between two peaks in Hz.[81] For complex **7b**, the SIR experiment was performed by saturating the resonance at 2.55 ppm, then following the exchange with the resonance at 2.95 ppm, corresponding to the CH group of the isopropyl moiety. These resonances were unambiguously assigned using a combination of COSY, TOCSY, NOESY, HSQC, and HMBC experiments. Unfortunately, the latter resonance overlaps with the peaks of the meta and para protons of the bridging toluene. This was corrected by subtracting 3/5 of the value for each data point, since the signal of interest integrates for 2 H atoms and the signals for the meta and para hydrogens of toluene integrate to 3 H atoms.

Crystallographic Analysis. X-ray structural determinations were performed on a Bruker SMART 1000 or SMART APEX diffractometer. Both are 3-circle diffractometers that couple a CCD detector[84] with a sealed-tube source of monochromated Mo Ka radiation (λ = 0.71073 Å). A crystal of appropriate size was coated in Paratone-N oil and mounted on a Kapton loop. The loop was transferred to the diffractometer, centered in the beam, and cooled by a nitrogen flow low-temperature apparatus that had been previously calibrated by a thermocouple placed at the same position as the crystal. Preliminary orientation matrices and cell constants were determined by collection of 60 10 s frames, followed by spot integration and least-

squares refinement. The reported cell dimensions were calculated from all reflections with $I > 10\ \sigma$. The data were corrected for Lorentz and polarization effects; no correction for crystal decay was applied. An empirical absorption correction based on comparison of redundant and equivalent reflections was applied using SADABS.[85] All software used for diffraction data processing and crystal structure solution and refinement are contained in the APEX2 program suite (Bruker AXS, Madison, WI).[86] Thermal parameters for all nonhydrogen atoms were refined anisotropically. For all structures, $R_1 = \sum(|F_o| - |F_c|)/\sum(|F_o|)$; $wR_2 = [\sum\{w(F_o^2 - F_c^2)^2\}/\sum\{w(F_o^2)^2\}]^{1/2}$. Thermal ellipsoid plots were created using the ORTEP-3 software package and POV ray.[87]

Nb $L_{3,2}$-Edge XANES Measurements. Sample preparation methodology was similar to that utilized previously.[88,89] In an argon-filled glovebox, each sample was ground in a mortar and pestle, and the particles were transferred to a Si_3N_4 window (100 nm, Silson). A second window was placed over the sample to sandwich the particles, and the windows were sealed together using epoxy. Single-energy images and Nb $L_{3,2}$-edge XANES spectra (Figure S21) were acquired using the STXM instrument at the Advanced Light Source beamline 5.3.2.1, which is operated in top-off mode at 500 mA, in a ~0.75 atm He-filled chamber.[90] This bending magnet beamline performs well with X-ray photons up to 2500 eV, which includes the Nb L_3- and L_2-edges (approximately 2370 and 2465 eV, respectively). Prior to each measurement, an energy calibration was performed at the Si K-edge for Si (1838.90 eV). For these measurements, the X-ray beam was focused with a zone plate onto the sample, and the transmitted light was detected. All measurements were performed using a 25 nm zone plate, and dwell times were ~10 ms per pixel. To quantify the absorbance signal, the measured transmitted intensity (I) was converted to optical density using Beer–Lambert's law: $OD = \ln(I/I_0) = \mu\rho d$, where I_0 is the incident photon flux intensity, d is the sample thickness, and μ and ρ are the mass absorption coefficients and density of the sample material, respectively. Incident beam intensity was measured through the sample-free region of the Si_3N_4 windows. Regions of particles with an absorption of >1.5 OD were omitted to ensure the spectra were in the linear regime of the Beer–Lambert law. The energy resolution (fwhm) was estimated at 1.0 eV.[90] During the STXM experiment, particles showed no signs of radiation damage, and each spectrum was reproduced from multiple independent particles. Positions of the L_3- and L_2-edge peak maxima were determined from the first derivative of the experimental spectra.

In order to evaluate d orbital occupancies from the Nb $L_{3,2}$ edge spectra, white line intensities must be isolated from the postedge regions beyond the absorption thresholds and normalized. This was achieved using IGOR 6.0 through a modification to an empirical procedure that was described in detail by Pearson and co-workers.[91] First, a straight line was fit to the pre-edge region (<2350 eV) and subtracted from the experimental data to eliminate the background of the spectrum. Postedge spectral intensity that was not a component of the $L_{3,2}$ white lines was modeled by fitting two additional lines to approximately 50 eV regions after the L_3 and L_2 absorption thresholds. The lines were extrapolated to span the full spectrum, and the integrated area under the lines at energies above the L_3 or L_2 edge maxima was subtracted from the total L_3 and L_2 edge intensities. Continuum intensity was determined by integrating over a 55 eV region of the spectrum beginning 30 eV above the energy of the L_3-edge maximum.[92] Normalized Nb $L_{3,2}$-edge intensities were calculated by dividing the total $L_{3,2}$-edge intensity by the continuum intensity.

■ ASSOCIATED CONTENT

Supporting Information

Details concerning NMR spectroscopy, X-ray structures, electronic spectroscopy, XANES and DFT calculations. This information is available free of charge via the Internet at http://pubs.acs.org.

■ AUTHOR INFORMATION

Corresponding Author

john.arnold@berkeley.edu

Notes

The authors declare no competing financial interest.

■ ACKNOWLEDGMENTS

We thank the AFOSR (grant no. FA9550-11-1-0008) for financial support, and Prof. Richard Andersen, Dr. Odile Eisenstein, Dr. Nikolas Kaltsozannis, Dr. Henry S. La Pierre, Benjamin M. Kriegel, and Mark Abubekerov for helpful discussions. T.L.G. is grateful to the UCB Department of Chemistry for the Howard W. Crandall Fellowship. The X-ray absorption work was supported by the Division of Chemical Sciences, Geosciences, and Biosciences, Office of Basic Energy Sciences, U.S. Department of Energy at LBNL (contract DE-AC02-05CH11231) and under the Heavy Element Chemistry Program at LANL (operated by Los Alamos National Security, LLC, for the National Nuclear Security Administration; contract DE-AC52-06NA25396). The X-ray absorption work was also supported at LANL by Glenn T. Seaborg Institute Postdoctoral Fellowships (S.G.M.), and at the ALS by the Director, Office of Science, Office of Basic Energy Sciences, of the U.S. Department of Energy under contract no. DE-AC02-05CH11231.

■ REFERENCES

(1) Muertterties, E. L.; Bleek, J. R.; Wucherer, E. J.; Albright, T. A. *Chem. Rev.* **1982**, *82*, 499.

(2) Cassani, M. C.; Gun'ko, Y. K.; Hitchcock, P. B.; Lappert, M. F.; Laschi, F. *Organometallics* **1999**, *18*, 5539.

(3) Bochkarev, M. N. *Chem. Rev.* **2002**, *102*, 2089.

(4) Duff, A. W.; Jonas, K.; Goddard, R.; Kraus, H. J.; Krueger, C. *J. Am. Chem. Soc.* **1983**, *105*, 5479.

(5) Krieck, S.; Görls, H.; Yu, L.; Reiher, M.; Westerhausen, M. *J. Am. Chem. Soc.* **2009**, *131*, 2977.

(6) Cotton, F. A.; Kibala, P. A; Wojtczak, W. A. *J. Am. Chem. Soc.* **1991**, *113*, 1462.

(7) Troyanov, S. I.; Meetsma, A.; Teuben, J. H. *Inorg. Chim. Acta* **1998**, *271*, 180.

(8) Tsai, Y.-C.; Wang, P.-Y.; Chen, S.-A.; Chen, J.-M. *J. Am. Chem. Soc.* **2007**, *129*, 8066.

(9) Nikiforov, G. B.; Crewdson, P.; Gambarotta, S.; Korobkov, I.; Budzelaar, P. H. M. *Organometallics* **2007**, *26*, 48.

(10) Tsai, Y.-C.; Wang, P.-Y.; Lin, K.-M.; Chen, S.-A.; Chen, J.-M. *Chem. Commun.* **2008**, 205.

(11) Ni, C.; Ellis, B. D.; Fettinger, J. C.; Long, G. J.; Power, P. P. *Chem. Commun.* **2008**, 1014.

(12) Bénard, M.; Rohmer, M. M.; López, X.; Theopold, K. H. *Angew. Chem., Int. Ed.* **2008**, *47*, 5597.

(13) Fryzuk, M. D.; Love, J. B.; Rettig, S. J. *J. Am. Chem. Soc.* **1997**, *119*, 9071.

(14) Diaconescu, P. L.; Arnold, P. L.; Baker, T. A.; Mindiola, D. J.; Cummins, C. C. *J. Am. Chem. Soc.* **2000**, *122*, 6108.

(15) Diaconescu, P. L.; Cummins, C. C. *J. Am. Chem. Soc.* **2002**, *124*, 7660.

(16) Evans, W. J.; Kozimor, S. A.; Ziller, J. W.; Kaltsoyannis, N. *J. Am. Chem. Soc.* **2004**, *126*, 14533.

(17) Evans, W. J.; Traina, C. A.; Ziller, J. W. *J. Am. Chem. Soc.* **2009**, *131*, 17473.

(18) Mills, D. P.; Moro, F.; McMaster, J.; van Slageren, J.; Lewis, W.; Blake, A. J.; Liddle, S. T. *Nat. Chem* **2011**, *3*, 454.

(19) Huang, W.; Khan, S. I.; Diaconescu, P. L. *J. Am. Chem. Soc.* **2011**, *133*, 10410.

(20) Monreal, M. J.; Khan, S. I.; Kiplinger, J. L.; Diaconescu, P. L. *Chem. Commun.* **2011**, *47*, 9119.

(21) Patel, D.; Moro, F.; McMaster, J.; Lewis, W.; Blake, A. J.; Liddle, S. T. *Angew. Chem., Int. Ed.* **2011**, *50*, 10388.
(22) Diaconescu, P. L.; Cummins, C. C. *Inorg. Chem.* **2012**, *51*, 2902.
(23) Arnold, P. L.; Mansell, S. M.; Maron, L.; McKay, D. *Nat. Chem.* **2012**, *4*, 668.
(24) Mougel, V.; Camp, C.; Pécaut, J.; Copéret, C.; Laurent Maron, L.; Kefalidis, C. E; Mazzanti, M. *Angew. Chem., Int. Ed.* **2012**, *51*, 12280.
(25) Minasian, S. G.; Krinsky, J. L.; Arnold, J. *Chem.—Eur. J.* **2011**, *17*, 12234.
(26) Gianetti, T. L.; Tomson, N. C.; Arnold, J.; Bergman, R. G. *J. Am. Chem. Soc.* **2011**, *133*, 14904.
(27) Fei, P.; Khan, M. A.; Nicholas, L. M. *J. Am. Chem. Soc.* **1992**, *114*, 6579.
(28) Fryzuk, M. D.; Kozak, C. M.; Bowdridge, M. R.; Patrick, B. O.; Rettig, S. J. *J. Am. Chem. Soc.* **2002**, *124*, 8389.
(29) Kilgore, U. J.; Yang, X.; Tomaszewski, J.; Huffman, J. C.; Daniel J. Mindiola, D. J. *Inorg. Chem.* **2006**, *45*, 10712.
(30) Figueroa, J. S.; Cummins, C. C. *Dalton Trans.* **2006**, 2161.
(31) Hiromasa Tanaka, H.; Shiota, Y.; Matsuo, T.; Kawaguchi, H.; Yoshizawa, K. *Inorg. Chem.* **2009**, *48*, 3875.
(32) Tomson, N. C.; Arnold, J.; Bergman, R. G. *Organometallics* **2010**, *29*, 5010.
(33) Steffey, B. D.; Chesnut, R. W.; Kerschner, J. L.; Pellechia, P. J.; Fanwick, P. E.; Rothwell, I. P. *J. Am. Chem. Soc.* **1989**, *111*, 378.
(34) Labinger, J. A.; Schwartz, J. *J. Am. Chem. Soc.* **1975**, *97*, 1596.
(35) Roskamp, E. J.; Pedersen, S. F. *J. Am. Chem. Soc.* **1987**, *109*, 6551.
(36) Etienne, M.; Biasotto, F.; Mathieu, R.; Templeton, J. L. *Organometallics* **1996**, *15*, 1106.
(37) Antinolo, A.; Otero, A. *Organometallics* **1997**, *16*, 2601.
(38) Obora, Y.; Kimura, M.; Ohtake, T.; Tokunaga, M.; Tsuji, Y. *Organometallics* **2006**, *25*, 2097.
(39) Rothwell, I. P. *Chem. Commun.* **1997**, 1331.
(40) Yu, J. S.; Fanwick, P. E.; Rothwell, I. P. *J. Am. Chem. Soc.* **1990**, *112*, 8171.
(41) Yu, J. S.; Felter, L.; Potyen, M. C.; Clark, J. R.; Visciglio, V. M.; Fanwick, P. E.; Rothwell, I. P. *Organometallics* **1996**, *15*, 4443.
(42) Veige, A. S.; Slaughter, L. M.; Lobkovsky, E. B.; Wolczanski, P. T.; Matsunaga, N.; Decker, S. A.; Cundari, T. R. *Inorg. Chem.* **2003**, *42*, 6204.
(43) Figueroa, J. S.; Piro, N. A.; Mindiola, D. J.; Fickes, M. G.; Cummins, C. C. *Organometallics* **2010**, *29*, 5215.
(44) Tomson, N. C.; Yan, A.; Arnold, J.; Bergman, R. G. *J. Am. Chem. Soc.* **2008**, *130*, 11262.
(45) A diniobium bridged benzene was reported that exhibits a μ-η^2:η^2 structure: Veige, A. S.; Kleckley, T. S.; Chamberlin, R. M; Neithamer, D. R; Lee, C. E.; Wolczanski, P. T.; Lobkovsky, E. B.; Glassey, W. V. *J. Organomet. Chem.* **1999**, *591*, 194.
(46) Tomson, N. C.; Arnold, J.; Bergman, R. G. *Organometallics* **2010**, *29*, 2926.
(47) Churchill, M. R.; Chang, S. W. -Y *J. Chem. Soc., Chem. Commun.* **1974**, 248.
(48) Goldberg, S. Z.; Spivack, B. D.; Stanley, G.; Eisenberg, R.; Braitsch, D. M.; Miller, J. S.; Abkowitz, M. *J. Am. Chem. Soc.* **1977**, *99*, 110.
(49) Stollmaier, F.; Thewalt, U. *J. Organomet. Chem.* **1981**, *222*, 227.
(50) Thewalt, U.; Stollmaier, F. *Angew. Chem., Int. Ed.* **1982**, *21*, 133.
(51) Bandy, J. A.; Prout, K.; Cloke, F. G. N.; de Lemos, H. C.; Wallis, J. M. *J. Chem. Soc., Dalton Trans.* **1988**, 1475.
(52) Green, M. L. H.; O'Hare, D.; Watkin, J. G. *J. Chem. Soc., Chem. Commun.* **1989**, 698.
(53) Calderazzo, F.; Pampaloni, G.; Rocchi, L.; Strahle, J.; Wurst, K. *J. Organomet. Chem.* **1991**, *413*, 91.
(54) Calderazzo, F.; Englert, U.; Pampaloni, G.; Rocchi, L. *Angew. Chem., Int. Ed.* **1992**, *31*, 1235.
(55) Calderazzo, F.; Gingl, F.; Pampaloni, G.; Rocchi, L.; Strahle, J. *Chem. Ber.* **1992**, *125*, 1005.
(56) Calderazzo, F.; De Benedetto, G. E; Pampaloni, G.; Rocchi, L.; Englert, U. *J. Organomet. Chem.* **1993**, *462*, C10.
(57) Calderazzo, F.; Pampaloni, G.; Rocchi, L.; Englert, U. *Organometallics* **1994**, *13*, 252.
(58) Clark, D. L.; Gordon, J. C.; McFarlan, J. T.; Vincent-Hollis, R. L.; Watkin, J. G.; Zwick, B. D. *Ingor. Chem. Acta.* **1996**, *244*, 269.
(59) Tayebani, M.; Feghali, K.; Gambarotta, S.; Yap, G. *Organometallics* **1998**, *17*, 4282.
(60) Kesanli, B.; Fettinger, J.; Eichhorn, B. *Angew. Chem., Int. Ed.* **2001**, *40*, 2300.
(61) Fryzuk, M. D.; Kozak, C. M.; Mehrkhodavandi, P.; Morello, L.; Patrick, B. O.; Rettig, S. J. *J. Am. Chem. Soc.* **2002**, *124*, 516.
(62) Sussman, V. J.; Ellis, J. E. *Angew. Chem., Int. Ed.* **2008**, *47*, 484.
(63) Plíva, J.; Johns, J. W. C.; Goodman, L. J. *Mol. Spectrosc* **1990**, *140*, 214.
(64) *Landolt-Bornstein: Numerical Data and Functional Relationships in Science and Technology*; Madelung, O., Ed.; Springer: Berlin, 1987; Vol. *15*.
(65) Maksić, J. B. *Int. J. Quantum Chem.* **1971**, *5*, 301.
(66) Bodner, G. M.; Todd, L. J. *Inorg Chem* **1974**, *13*, 360.
(67) *The Organometallic Chemistry of the Transition Metals*, 4th ed.; Crabtree, R. H., Ed.; John Wiley & Sons, Inc.: Hoboken NJ, 2005, p 87.
(68) Da Re, R. E; Kuehl, C. J.; Brown, M. G; Rocha, R. C.; Bauer, E. D.; John, K. D.; Morris, D. E; Shreve, A. P.; Sarrao, J. L. *Inorg. Chem.* **2003**, *42*, 5551.
(69) Pearson, D. H.; Ahn, C. C.; Fultz, B. *Phys. Rev. B* **1993**, *47*, 8471.
(70) Bach, D.; Schneider, R.; Gerthsen, D.; Verbeeck, J.; Sigle, W. *Microsc. Microanal.* **2009**, *15*, 505.
(71) Pearson, D. H.; Fultz, B.; Ahn, C. C. *Appl. Phys. Lett.* **1988**, *53*, 1405.
(72) Olszta, M. J.; Wang, J.; Dickey, E. C. *J. Microsc. (Oxford, U. K.)* **2006**, *224*, 233.
(73) Bach, D.; Stoermer, H.; Schneider, R.; Gerthsen, D.; Verbeeck, J. *Microsc. Microanal.* **2006**, *12*, 416.
(74) Bach, D.; Schneider, R.; Gerthsen, D. *Microsc. Microanal.* **2009**, *15*, 524.
(75) Tao, R.; Todorovic, R.; Liu, J.; Meyer, R. J.; Arnold, A.; Walkosz, W.; Zapol, P.; Romanenko, A.; Cooley, L. D.; Klie, R. F. *J. Appl. Phys.* **2011**, *110*, 124313.
(76) Solomon, E. I.; Lever, A. B. P. *Inorganic Electronic Structure and Spectroscopy*; John Wiley & Sons: Hoboken, NJ, 2006; Vol. *2*.
(77) Alaimo, P. J.; Peters, D. W.; Arnold, J.; Bergman, R. G. *J. Chem. Educ.* **2001**, *78*, 64.
(78) Feldman, J.; McLain, S. J.; Parthasarathy, A.; Marshall, W. J.; Calabrese, J. C.; Arthur, S. D. *Organometallics* **1997**, *16*, 1514.
(79) Budzelaar, P. H. M.; van Oort, A. B.; Orpen, A. G. *Eur. J. Inorg. Chem.* **1998**, *10*, 1485.
(80) Anderson, L. L.; Arnold, J.; Bergman, R. G. *J. Am. Chem. Soc.* **2005**, *127*, 14541.
(81) Amman, C.; Meier, P.; Merbach, A. E. *J. Magn. Reson.* **1982**, *46*, 319.
(82) Bain, A. D.; Cramer, J. A. *J. Magn. Reson. A* **1996**, *118*, 21.
(83) Mugridge, J. S.; Szigethy, G.; Bergman, R. G; Raymond, K. N *J. Am. Chem. Soc.* **2010**, *132*, 16256.
(84) *SMART: Area-Detector Software Package*; Brucker Analytic X-ray Systems: Madison, WI, 2001−2003.
(85) *SADABS: Bruker-Nonius Area Detector Scaling and Absorption*, V2.05; Brucker Analytic X-ray Systems: Madison, WI, 2003.
(86) Sheldrick, G. M. *Acta. Crystallogr. A* **2008**, *64*, 112.
(87) Farrugia, L. J. *J. Appl. Crystallogr.* **1997**, *30*, 565 Ed..
(88) Bradley, J. A.; Yang, P.; Batista, E. R.; Boland, K. S.; Burns, C. J.; Clark, D. L.; Conradson, S. D.; Kozimor, S. A.; Martin, R. L.; Seidler, G. T.; Scott, B. L.; Shuh, D. K.; Tyliszczak, T.; Wilkerson, M. P.; Wolfsberg, L. E. *J. Am. Chem. Soc.* **2010**, *132*, 13914.
(89) Minasian, S. G.; Krinsky, J. L.; Rinehart, J. D.; Copping, R.; Tyliszczak, T.; Janousch, M.; Shuh, D. K.; Arnold, J. *J. Am. Chem. Soc.* **2009**, *131*, 13767.

(90) Kilcoyne, A. L. D.; Ade, H.; Attwood, D.; Hitchcock, A. P.; McKean, P.; Mitchell, G. E.; Monteiro, P.; Tyliszczak, T.; Warwick, T. *AIP Conf. Proc.* **2010**, *1234*, 459.
(91) Pearson, D. H.; Ahn, C. C.; Fultz, B. *Phys. Rev. B* **1993**, *47*, 8471.
(92) Bach, D.; Schneider, R.; Gerthsen, D.; Verbeeck, J.; Sigle, W. *Microsc. Microanal.* **2009**, *15*, 505.